

CAD-VAE: Leveraging Correlation-Aware Latents for Comprehensive Fair Disentanglement

Chenrui Ma¹, Xi Xiao², Tianyang Wang², Xiao Wang³, Yanning Shen^{1*}

¹University of California, Irvine, Irvine, CA 92697, USA

²University of Alabama at Birmingham, Birmingham, AL 35294, USA

³Oak Ridge National Laboratory, Oak Ridge, TN 37830, USA

Abstract

While deep generative models have significantly advanced representation learning, they may inherit or amplify biases and fairness issues by encoding sensitive attributes alongside predictive features. Enforcing strict independence in disentanglement is often unrealistic when target and sensitive factors are naturally correlated. To address this challenge, we propose **CAD-VAE** (Correlation-Aware Disentangled VAE), which introduces a correlated latent code to capture the information shared between the target and sensitive attributes. Given this correlated latent, our method effectively separates overlapping factors without extra domain knowledge by directly minimizing the conditional mutual information between target and sensitive codes. A relevance-driven optimization strategy refines the correlated code by efficiently capturing essential correlated features and eliminating redundancy. Extensive experiments on benchmark datasets demonstrate that CAD-VAE produces fairer representations, realistic counterfactuals, and improved fairness-aware image editing. Source code is available : <https://github.com/merry7cherry/CAD-VAE>

Introduction

Deep generative models have achieved remarkable success in capturing complex data distributions for applications ranging from image synthesis (Bai et al. 2024; Ma et al. 2025c,b) to video generation (Montanaro et al. 2024). In particular, variational autoencoders (VAEs)(Higgins et al. 2017; Kingma and Welling 2022; Mathieu et al. 2019; Ma et al. 2025a) have provided a principled approach to representation learning, where data are encoded into compact latent variables that effectively capture meaningful factors of variation. However, while these latent representations have enabled impressive performance in numerous tasks, concerns about fairness have emerged, as models can inadvertently learn and amplify biases present in training data(Jang and Wang 2024).

Such fairness issues arise when the target label and sensitive label become entangled due to societal or dataset biases (Lahoti et al. 2020; Liu et al. 2021). To address these problems, existing methods commonly fall into two categories. Invariant learning techniques aim to remove sensitive attributes from the learned representation, often via adversarial training or additional regularization (Lahoti et al. 2020;

Roy and Boddeti 2019). By contrast, disentanglement approaches encourage the model to partition its latent space into separate codes for target and sensitive information, seeking statistical independence among them (Creager et al. 2019; Liu, Sun, and Zhao 2023). Although these solutions have made progress, they typically assume minimal correlation between target and sensitive factors or enforce strict separation via mutual information penalties (Chen et al. 2018). However, multiple works (Jang and Wang 2024; Park et al. 2020) have demonstrated that achieving fully fair disentanglement is fundamentally impossible under realistic conditions. First, many datasets contain unwanted correlations between the target label and sensitive attributes due to societal bias, making it infeasible to preserve all predictive cues while completely discarding sensitive information (Dressel and Farid 2018). Second, certain features inherently influence both target and sensitive attributes, so perfectly partitioning features into disjoint latent spaces is unachievable without compromising prediction accuracy (Kohavi 1996). In these circumstances, any attempt at full disentanglement faces an inevitable trade-off between fairness and utility.

A natural way to handle this correlation is to explicitly model how target and sensitive attributes overlap. For instance, some methods rely on causal graphs to separate task-relevant features and capture their relationships with sensitive variables (Kim et al. 2021; Sánchez-Martin, Rateike, and Valera 2022; Zhu et al. 2023; Hwa et al. 2024). However, constructing such graphs requires extensive domain knowledge, which is often challenging to acquire in real-world scenarios.

Motivated by the limitations of existing methods, an correlated latent code is introduced to capture the shared information between target and sensitive attributes. Our approach advances existing methods (Jang and Wang 2024; Park et al. 2020) by a directly minimizing conditional mutual information mechanism to achieve disentanglement and an explicit relevance learning strategy to learn the correlated latent code efficiently and properly, as summarized follow:

1. We propose a novel correlation-aware representation learning framework that directly minimizes the conditional mutual information between target and sensitive property, conditioned on the correlated latent code, effectively addressing the conflict between predictive objectives and disentanglement.
2. We introduce an explicit relevance-driven optimization

*Corresponding author: yannings@uci.edu.

Copyright © 2026, Association for the Advancement of Artificial Intelligence (www.aaai.org). All rights reserved.

strategy that precisely regulates the correlated latent code, ensuring it captures only the essential shared information without extra domain knowledge.

3. We validate our approach through comprehensive experiments on multiple benchmark datasets, demonstrating its superiority in achieving correlation-aware disentanglement, enhancing fair prediction performance, and improving both counterfactual generation and fairness-aware image editing, as well as its broad applicability in the context of Vision-Language Models (VLM).

Related Work

Fair Disentanglement Learning

Fair disentanglement methods aim to separate representations into target-related and sensitive-related latent codes rather than directly removing sensitive information (Liu, Sun, and Zhao 2023; Madras et al. 2018; Xu et al. 2018; Wang et al. 2024). Early works such as β -VAE (Higgins et al. 2017) and FactorVAE (Kim and Mnih 2018) introduced mechanisms for semantic decomposition of latent factors, with FactorVAE promoting independence across dimensions by reducing total correlation. Building on this foundation, FairFactorVAE (Liu, Sun, and Zhao 2023) further restricts sensitive leakage within the disentanglement process.

Subsequent studies refine these ideas by emphasizing flexible or guided decomposition. FFVAE (Creager et al. 2019) adapts latent structures to better isolate sensitive attributes, while GVAE (Ding et al. 2020) employs adversarial constraints to suppress unwanted information. Other strategies incorporate structural priors such as orthogonality in ODVAE (Sarhan et al. 2020) or distance-covariance minimization in FairDisCo (Liu et al. 2022). These approaches collectively illustrate progress in disentanglement, yet also reveal the challenge of fully separating target and sensitive information when these factors are inherently correlated.

Correlation-Aware Learning

Despite advancements in disentanglement, perfect independence between latent codes is difficult to achieve due to natural correlations between sensitive and target attributes (Mehrabi et al. 2021; Jang and Wang 2024). For example, facial attributes in CelebA (Liu et al. 2015), such as “mustache,” correlate with both gender and attractiveness, complicating clean separation.

Correlation-aware learning frameworks seek to address this by leveraging causal graphs to categorize latent variables according to their relationships with sensitive attributes (Kim et al. 2021; Sánchez-Martin, Rateike, and Valera 2022; Zhu et al. 2023; Hwa et al. 2024). However, causal-graph construction requires strong domain knowledge, and inaccurate assumptions may hinder independence (Jang and Wang 2024). FADES (Jang and Wang 2024) mitigates this dependency by grouping samples across attributes to approximate conditional mutual information and capture shared sensitive-relevant structure. While effective in some contexts, this indirect method may still allow leakage and offers limited control over relevance allocation. These limitations motivate approaches that directly optimize conditional independence

with explicit guidance for balancing sensitive-relevant information.

Counterfactual Fairness

Counterfactual fairness (CF) evaluates whether predictions remain stable when sensitive attributes are hypothetically altered (Kusner et al. 2017). Causal inference is widely used to generate counterfactual instances (Zhou et al. 2024; Jung et al. 2025; Zhu et al. 2023; Chiappa 2019; Wu, Zhang, and Wu 2019), enabling comparisons between factual and hypothetical outcomes.

Graph-based CF models (Kim et al. 2021; Li et al. 2025) rely on predefined causal structures to produce realistic counterfactuals, but these structures demand precise domain knowledge; inaccurate models may lead to implausible counterfactuals, such as depicting a female subject with a mustache. Although CF offers strong theoretical grounding, its reliance on domain expertise limits practical deployment. To overcome this challenge, our approach introduces a correlated latent code with an explicit relevance-learning mechanism, allowing the model to autonomously learn attribute relationships and enhance counterfactual fairness without external causal assumptions.

Preliminary

Conditional Independence and Mutual Information

Proposition 1 (Conditional Independence). *Let A , B , and C be random variables. We say that A is **conditionally independent** of B given C , denoted $A \perp B | C$, if and only if their conditional joint probability distribution factorizes as follows:*

$$p(A, B | C) = p(A | C)p(B | C). \quad (1)$$

Directly measuring the degree of conditional independence by computing the divergence between the two sides of Eq. (1) is often intractable in practice, especially in the context of deep learning models where the underlying distributions are complex and high-dimensional. Instead, a common and more tractable approach is to use an information-theoretic surrogate measure.

Definition 1 (Conditional Mutual Information). *The **Conditional Mutual Information** (CMI) between two random variables A and B given a third random variable C measures the expected amount of information that A and B share, conditioned on C . It is defined as the expected Kullback-Leibler (KL) divergence between the conditional joint distribution and the product of the conditional marginal distributions:*

$$I(A; B | C) = \mathbb{E}_{p(C)} \left[D_{\text{KL}} \left(p(A, B | C = c) \| p(A | C = c)p(B | C = c) \right) \right]. \quad (2)$$

This can be expressed over the entire distribution of C as:

$$I(A; B | C) = \int D_{\text{KL}} \left(p(A, B | C) \| p(A | C)p(B | C) \right) dp(C). \quad (3)$$

CMI provides a principled way to measure conditional dependence due to its fundamental properties.

Lemma 1 (Properties of CMI). *Conditional mutual information is non-negative, i.e., $I(A; B | C) \geq 0$. Furthermore,*

$I(A; B | C) = 0$ if and only if A and B are conditionally independent given C ($A \perp B | C$). See Appendix 1 for a detailed proof.

Lemma 2 (Symmetry of CMI). *Conditional mutual information is symmetric in its primary arguments:*

$$I(A; B | C) = I(B; A | C). \quad (4)$$

Variational Autoencoder

A Variational Autoencoder (VAE) (Kingma and Welling 2022) is a generative model that learns a latent representation of data. It uses an **encoder** network, $q_\phi(z | x)$, to map an input sample x to a latent distribution, and a **decoder** network, $p_\theta(x | z)$, to reconstruct the input from a latent sample z .

The model is trained by minimizing the negative Evidence Lower Bound (ELBO):

$$\mathcal{L}_{\text{VAE}}(\theta, \phi) = \underbrace{\mathbb{E}_{q_\phi(z|x)}[-\log p_\theta(x|z)]}_{\text{Reconstruction Loss}} + \underbrace{\text{KL}\left(q_\phi(z|x) \parallel p_\theta(z)\right)}_{\text{KL Divergence}}, \quad (5)$$

where the first term measures reconstruction accuracy and the second term is a regularizer that pushes the learned latent distribution $q_\phi(z | x)$ towards a prior $p_\theta(z)$, which is typically a standard Gaussian $\mathcal{N}(0, I)$.

Total Correlation Loss

To enforce statistical independence among latent variables, **FactorVAE** (Kim and Mnih 2018) introduces a penalty on the **Total Correlation** (TC). TC is the Kullback-Leibler (KL) divergence between the aggregate posterior, $q(z)$, and the product of its marginals, $\prod_j q(z_j)$:

$$L_{TC} = \text{KL}\left(q(z) \parallel \prod_j q(z_j)\right) \quad (6)$$

As this term is intractable to compute directly, it is approximated using a discriminator, D , which is trained to distinguish between samples from $q(z)$ and samples from the product of marginals (approximated by permuting dimensions across a batch). The encoder, in turn, is trained to minimize the following adversarial loss, thereby fooling the discriminator and reducing the TC:

$$L_{TC} \approx \mathbb{E}_{q(z)} \left[\log \frac{D(z)}{1 - D(z)} \right] \quad (7)$$

Method

We first present the problem definition, model components, and architecture, which serve as crucial foundations for the subsequent sections.

CAD-VAE

Let $\mathcal{D} = \{(x_i, y_i, s_i)\}_{i=1}^N$ denote a dataset consisting of triplets, where x_i denotes an input sample (e.g., an image), y_i is the label of x_i corresponding to target property Y , and s_i is the label corresponding to the sensitive property S . The value range of Y and S is \mathcal{Y} and \mathcal{S} , respectively, i.e., $y \in \mathcal{Y}$ and $s \in \mathcal{S}$.

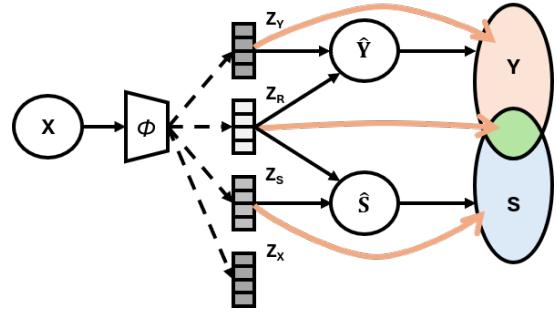


Figure 1: **Illustration of the data flow.** The orange lines connect the information in the observed space and their corresponding latent codes.

As discussed in Introduction, correlated information between the target attribute Y and the sensitive attribute S is pervasive in disentanglement learning. To address this, we introduce an additional latent code z_R to explicitly model this correlated information.

The goal is to learn a latent representation that factorizes the information relevant to Y , the information relevant to S , the shared information between Y and S , and the background or irrelevant factors. As defined below:

- z_X : captures task-irrelevant information.
- z_Y : encodes the information strongly correlated with Y .
- z_S : encodes the information strongly correlated with S .
- z_R : represents the *shared* information between Y and S .

Hence, for a single observation, the corresponding latent variable set is $z := (z_X, z_Y, z_S, z_R)$.

The latent code z_R isolates the overlapping information between Y and S , which allows the primary latent codes z_Y and z_S to remain free of unwanted correlations while preserving the model's predictive power (Creager et al. 2019; Kim et al. 2021; Jang and Wang 2024). From a causal perspective as illustrated in Figure 1, if Y and S are conditionally independent given z_R , then z_R acts as their common cause, thereby promoting the independence of z_Y and z_S .

To learn such latent code, we employ the Variational Autoencoder (VAE) framework as our backbone. The model is trained to minimize the negative ELBO, \mathcal{L}_{VAE} , as defined in Eq. (5).

In addition, we introduce four classifiers to enforce different constraints, including:

- Enforcing z_Y and z_S to capture sufficient information ensures that attributes Y and S can be recovered correspondingly in alignment with z_R .
- Eliminating information leakage (see in subsequent section)
- Encouraging z_R encapsulate only the correlated information $Y \cap S$ (see in subsequent section)

Here, we first present the training method and loss function of each classifier.

- $f_y(z_Y, z_R)$ is a classifier that predicts \hat{y} from (z_Y, z_R) ;
- $f_s(z_S, z_R)$ is a classifier that predicts \hat{s} from (z_S, z_R) ;

- $f_{y_op}(z_S)$ is an *opponent* classifier that attempts to predict \hat{y} from z_S ;
- $f_{s_op}(z_Y)$ is an *opponent* classifier that attempts to predict \hat{s} from z_Y .

Let $\omega_y, \omega_s, \omega_{y_op}$, and ω_{s_op} denote the parameters of these four classifiers, respectively.

We define

$$\min_{\phi, \omega_y} [\mathcal{L}_y(\omega_y, \phi)] = \mathbb{E}_{(x, y) \sim \mathcal{D}} [-\log f_y(\hat{y} | z_Y, z_R)], \quad (8)$$

where z_Y and z_R are sampled from the encoder $q_\phi(z | x)$: $(z_Y, z_R) \sim q_\phi(z | x)$. The parameters ω_y and the encoder parameters ϕ are jointly updated to reduce the cross-entropy in (8), ensuring that (z_Y, z_R) carry sufficient information about Y . Similarly, the classifier $f_s(z_S, z_R)$ predicts s :

$$\min_{\phi, \omega_s} [\mathcal{L}_s(\omega_s, \phi)] = \mathbb{E}_{(x, s) \sim \mathcal{D}} [-\log f_s(\hat{s} | z_S, z_R)]. \quad (9)$$

To measure the information leakage, we introduce:

$$\min_{\omega_{y_op}} [\mathcal{L}_{y_op}(\omega_{y_op}; \phi)] = \mathbb{E}_{(x, y) \sim \mathcal{D}} [-\log f_{y_op}(\hat{y} | z_S)], \quad (10)$$

where $z_S \sim q_\phi(z | x)$ is produced by the frozen encoder i.e ϕ is *not* updated during the minimization of (10); this network is trained to detect any Y -relevant information that may unintentionally exist in z_S . Analogously, the classifier $f_{s_op}(z_Y)$ aims to predict s given z_Y :

$$\min_{\omega_{s_op}} [\mathcal{L}_{s_op}(\omega_{s_op}; \phi)] = \mathbb{E}_{(x, s) \sim \mathcal{D}} [-\log f_{s_op}(\hat{s} | z_Y)]. \quad (11)$$

Likewise, ϕ is fixed, and only ω_{s_op} is updated when minimizing (11).

To achieve correlation-aware disentanglement learning, we propose directly minimizing the conditional mutual information between z_Y and z_S with respect to their corresponding opposite attributes S and Y , conditioned on z_R . This approach is complemented by an explicit relevance learning strategy that constrains z_R to effectively capture shared information between Y and S while avoiding redundant information. Detailed explanations of these strategies are provided in following section.

Conditional Independence for Disentanglement

Our fairness objective is to achieve independence between z_Y and z_S by enforcing conditional independence between their respective predictions, \hat{Y} and \hat{S} , given the shared latent code z_R . The predictions are generated by classifiers: $\hat{Y} = f_y(z_Y, z_R)$ and $\hat{S} = f_s(z_S, z_R)$. This objective is formally expressed as $\hat{Y} \perp \hat{S} | z_R$. Following **Proposition 1**, this conditional independence is equivalent to the factorization of the conditional joint distribution:

$$p_\theta(\hat{Y}, \hat{S} | z_R) = p_\theta(\hat{Y} | z_R)p_\theta(\hat{S} | z_R). \quad (12)$$

As noted in the Preliminary section, directly minimizing the divergence between the distributions in Eq. (12) is generally intractable. We therefore adopt an information-theoretic

approach and minimize the Conditional Mutual Information (CMI), $I_\phi(\hat{Y}; \hat{S} | z_R)$, as a tractable surrogate objective.

From **Definition 1**, the CMI is the expected KL divergence over z_R :

$$\begin{aligned} I_\phi(\hat{Y}; \hat{S} | z_R) &= \\ \int D_{\text{KL}}(p_\theta(\hat{Y}, \hat{S} | z_R) \| p_\theta(\hat{Y} | z_R)p_\theta(\hat{S} | z_R)) dP_{z_R}. \end{aligned} \quad (13)$$

According to **Lemma 1**, minimizing $I_\phi(\hat{Y}; \hat{S} | z_R)$ to zero is equivalent to enforcing the conditional independence defined in Eq. (12). Furthermore, leveraging the symmetry property from **Lemma 2**, we note that $I_\phi(\hat{Y}; \hat{S} | z_R) = I_\phi(\hat{S}; \hat{Y} | z_R)$. Thus, minimizing this CMI ensures that any undesired dependence between \hat{Y} and \hat{S} not explained by z_R is removed.

Direct Minimization of Conditional Mutual Information

While FADES (Jang and Wang 2024) minimizing CMI (13) through approximation $I_\phi(\hat{Y}; S | z_R)$:

$$\min_{\phi} [I_\phi(\hat{Y}; S | z_R)] = \min_{\phi} [H_\phi(\hat{Y} | z_R) - H_\phi(\hat{Y} | S, z_R)]$$

by reducing CMI through ground truth-based sample grouping, its reliance on batch-level sampling introduces instability.

In contrast, our method directly minimizes CMI (13) via a principled information-theoretic approach, providing a more robust and stable disentanglement process by avoiding sampling variance and reducing dependency on batch-specific dynamics. To achieve CI as (12), we propose directly minimizing:

$$\min_{\phi} [I_\phi(\hat{Y}; \hat{S} | z_R) + I_\phi(\hat{S}; \hat{Y} | z_R)], \quad (14)$$

where:

$$I_\phi(\hat{Y}; \hat{S} | z_R) = H_\phi(\hat{Y} | z_R) - H_\phi(\hat{Y} | \hat{S}, z_R), \quad (15)$$

$H_\phi(* | *)$ stands for the conditional entropy. Incorporating $\hat{S} = f_s(z_S, z_R)$, we have:

$$\begin{aligned} I_\phi(\hat{Y}; \hat{S} | z_R) &= H_\phi(\hat{Y} | z_R) - H_\phi(\hat{Y} | \hat{S}, z_R) \\ &= H_\phi(\hat{Y} | z_R) - H_\phi(\hat{Y} | f_s(z_S, z_R), z_R) \\ &= H_\phi(\hat{Y} | z_R) - H_\phi(\hat{Y} | z_S, z_R) \\ &= I_\phi(\hat{Y}; z_S | z_R), \end{aligned} \quad (16)$$

from the same transformation (see detailed derivation in *Appendix 2*):

$$\begin{aligned} I_\phi(\hat{S}; \hat{Y} | z_R) &= I_\phi(\hat{S}; z_Y | z_R) \\ &= H_\phi(\hat{S} | z_R) - H_\phi(\hat{S} | z_Y, z_R). \end{aligned} \quad (17)$$

Therefore, with the introduction of the correlated latent code z_R that captures all relevant information between \hat{Y} and \hat{S} :

$$\begin{aligned} \min_{\phi} [I_\phi(\hat{Y}; \hat{S} | z_R) + I_\phi(\hat{S}; \hat{Y} | z_R)] \\ \equiv \min_{\phi} [I_\phi(\hat{Y}; z_S | z_R) + I_\phi(\hat{S}; z_Y | z_R)]. \end{aligned} \quad (18)$$

For the minimization of $I_\phi(\hat{Y}; z_S | z_R)$, as shown in (16), since z_R is given as a condition, we can consider this CMI formula as a function where the independent variable is z_S and the dependent variable is \hat{Y} , as shown as:

$$\mathcal{L}_{\hat{Y}}(z_S) = H_\phi(\hat{Y} | z_R) - H_\phi(\hat{Y} | z_S, z_R), \quad (19)$$

where z_R is determined here, $H_\phi(\hat{Y} | z_R)$ is a constant, henceforth we need to minimize $-H_\phi(\hat{Y} | z_S, z_R)$. Empirically, we directly minimize the lower bound of it: $-H_\phi(\hat{Y} | z_S)$, since: $-H_\phi(\hat{Y} | z_S, z_R) \geq -H_\phi(\hat{Y} | z_S)$. Symmetrically, the minimization of $I_\phi(\hat{S}; z_Y | z_R)$ shown in (17) is the same concept, see *Appendix 2* for detailed derivation. In this optimization process, z_R is responsible for containing any correlation information between target attribute Y and sensitive attribute S .

After these simplifications, we introduce the CMI loss to minimize (14):

$$\min_{\phi} [\mathcal{L}_{\text{CMI}}(\omega_{y,op}; \omega_{s,op}; \phi)] = -(H_\phi(\hat{Y} | z_S) + H_\phi(\hat{S} | z_Y)), \quad (20)$$

where only update encoder parameters ϕ . Utilizing opponent classifier $f_{y,op}(z_S)$, the entropy term calculation are shown as below:

$$\begin{aligned} H_\phi(\hat{Y} | z_S) &= \mathbb{E}_{q_\phi(z_S | x)} \left[-\sum_{\hat{y} \in \mathcal{Y}} p_\theta(\hat{y} | z_S) \log p_\theta(\hat{y} | z_S) \right] \\ &= \frac{1}{|B|} \sum_{i=1}^{|B|} \sum_{\hat{y} \in \mathcal{Y}} \left[-p_\theta(\hat{y} | z_S^{(i)}) \log p_\theta(\hat{y} | z_S^{(i)}) \right], \end{aligned} \quad (21)$$

where $p_\theta(\hat{y} | z_S^{(i)}) = f_{y,op}(z_S^{(i)})$. Here, $z_S^{(i)}$ denotes the z_S sample from the i -th element in a mini-batch of size $|B|$; the distribution $q_\phi(z_S | x)$ is given by the encoder. Similar calculation to $H_\phi(\hat{S} | z_Y)$, see *Appendix 3* for completed calculation formula. During this optimization process, the opponent classifier parameters $\omega_{y,op}$ and $\omega_{s,op}$ are frozen.

Learning Relevance Between Target And Sensitive Information

To encourage z_R capture and only capture the shared information relevant to target property and sensitive property, as well as z_Y, z_S capture main information of Y and S attributes respectively, we propose to maximize the conditional mutual information as Learning Relevance Information loss:

$$\min_{\phi} [\mathcal{L}_{\text{LRI}}(\omega_y; \omega_s; \phi)] = -(I_\phi(\hat{Y}; Y | z_R) + I_\phi(\hat{S}; S | z_R)), \quad (22)$$

where:

$$I_\phi(\hat{Y}; Y | z_R) = H_\phi(\hat{Y} | z_R) - H_\phi(\hat{Y} | Y, z_R), \quad (23)$$

$$I_\phi(\hat{S}; S | z_R) = H_\phi(\hat{S} | z_R) - H_\phi(\hat{S} | S, z_R), \quad (24)$$

$H_\phi(*)$ stands for the conditional entropy. Maximizing $H_\phi(\hat{Y} | z_R), H_\phi(\hat{S} | z_R)$ avoid z_R capture all information of Y or S solely, which will lead to the Information Bottleneck phenomenon(Jang and Wang 2024; Creager et al. 2019; Kim and Mnih 2018) i.e z_R capture all the information about target attribute Y and sensitive attribute S : $Y \cup S$, degenerating

disentanglement performance. On the other hand, minimizing $H_\phi(\hat{Y} | Y, z_R)$ and $H_\phi(\hat{S} | S, z_R)$ enforce z_R determine \hat{Y} or \hat{S} only within each Y or S subgroup, so that encourage z_R capture information both relevant to Y and S : $Y \cap S$.

In contrast to FADES(Jang and Wang 2024), which exhibits a conflict between the disentanglement term and the regularization term, our method achieves orthogonality between CMI (20) and LRI (22), ensuring fair disentanglement while preserving robust representations. See *Appendix 5* for details.

For entropy calculation of $H_\phi(\hat{Y} | z_R)$, We approximate $p_\theta(\hat{y} | z_R)$ by marginalizing over z_Y :

$$\begin{aligned} p_\theta(\hat{y} | z_R^{(k)}) &= \mathbb{E}_{p(x)} \left[\mathbb{E}_{q_\phi(z_Y | x)} \left[p_\theta(\hat{y} | z_Y, z_R^{(k)}) \right] \right] \\ &\approx \frac{1}{|B|} \sum_{i=1}^{|B|} p_\theta(\hat{y} | z_Y^{(i)}, z_R^{(k)}), \end{aligned} \quad (25)$$

where $p_\theta(\hat{y} | z_Y^{(i)}, z_R^{(k)}) = f_y(z_Y^{(i)}, z_R^{(k)})$, then

$$\begin{aligned} H_\phi(\hat{Y} | z_R) &= \mathbb{E}_{q_\phi(z_R | x)} \left[-\sum_{\hat{y} \in \mathcal{Y}} p_\theta(\hat{y} | z_R) \log p_\theta(\hat{y} | z_R) \right] \\ &= \frac{1}{|B|} \sum_{i=1}^{|B|} \sum_{\hat{y} \in \mathcal{Y}} \left[-p_\theta(\hat{y} | z_R^{(i)}) \log p_\theta(\hat{y} | z_R^{(i)}) \right]. \end{aligned} \quad (26)$$

As for the calculation of conditional entropy term $H_\phi(\hat{Y} | Y, z_R)$, we regard known condition Y as attribute to grouping samples in a mini-batch of size $|B|$, and calculate the entropy term by marginalizing over z_Y within each group, $p_\theta(\hat{y} | z_R, y)$ can be computed for $z_R^{(k)}$ sampled from an instance $x^{(k)} \in B_y$ as:

$$\begin{aligned} p_\theta(\hat{y} | z_R^{(k)}, y) &= \mathbb{E}_{p(x | Y=y)} \left[\mathbb{E}_{q_\phi(z_Y | x)} \left[p_\theta(\hat{y} | z_Y, z_R^{(k)}) \right] \right] \\ &\approx \frac{1}{|B_y|} \sum_{i=1}^{|B_y|} p_\theta(\hat{y} | z_Y^{(i)}, z_R^{(k)}), \end{aligned} \quad (27)$$

where B_y denotes a subset of the batch with $Y = y$. Then the conditional entropy can be computed as:

$$\begin{aligned} H_\phi(\hat{Y} | Y, z_R) &= \mathbb{E}_{(x,y) \sim \mathcal{D}} \left[\mathbb{E}_{q_\phi(z_R | x)} \left[-\sum_{\hat{y} \in \mathcal{Y}} p_\theta(\hat{y} | z_R, y) \log p_\theta(\hat{y} | z_R, y) \right] \right] \\ &= \frac{1}{|B|} \sum_{y \in \mathcal{Y}} \sum_{i=1}^{|B_y|} \sum_{\hat{y} \in \mathcal{Y}} \left[-p_\theta(\hat{y} | z_R^{(i)}, y) \log p_\theta(\hat{y} | z_R^{(i)}, y) \right]. \end{aligned} \quad (28)$$

The calculation of $H_\phi(\hat{S} | z_R)$ and $H_\phi(\hat{S} | S, z_R)$ are similar to $H_\phi(\hat{Y} | z_R)$, $H_\phi(\hat{Y} | Y, z_R)$ respectively, see *Appendix 3* for completed calculation formula. Plugging these estimates(26)(28) back into (22), shared feature between Y and S will be learned in z_R while getting rid of Information Bottleneck phenomenon. Note that the classifier parameters ω_y and ω_s remain frozen when optimizing (22).

Table 1: **Evaluation of downstream classification tasks on various datasets from learned representation.** Best in **bold**, second in **red**.

Methods	Downstream Classification Performance						Color bias MNIST (Kim et al. 2019)		
	CelebA (Liu et al. 2015)			UTKFace (Zhang, Song, and Qi 2017)					
	Acc ↑	EOD ↓	DP ↓	Acc ↑	EOD ↓	DP ↓	Acc ↑	EOD ↓	DP ↓
FADES (Jang and Wang 2024) [CVPR’24]	0.918	0.034	0.135	0.812	0.059	0.139	0.769	0.058	0.086
GVAE (Ding et al. 2020) [CVPR’20]	0.919	0.047	0.131	0.819	0.204	0.197	0.748	0.064	0.131
FFVAE (Creager et al. 2019) [PMLR’19]	0.892	0.076	0.072	0.766	0.269	0.201	0.729	0.059	0.110
ODVAE (Sarhan et al. 2020) [ECCV’20]	0.886	0.039	0.103	0.736	0.165	0.210	0.689	0.051	0.038
FairDisCo (Liu et al. 2022) [KDD’22]	0.839	0.074	0.051	0.766	0.266	0.200	0.680	0.115	0.111
FairFactorVAE (Liu, Sun, and Zhao 2023)	0.914	0.055	0.136	0.720	0.096	0.134	0.707	0.055	0.110
CAD-VAE (Ours)	0.939	0.021	0.065	0.828	0.045	0.137	0.781	0.048	0.069
							0.984	0.076	0.108

Final Objective Function

To integrate the above components into a coherent training framework, we employ the two-step optimization strategy defined in (29) and (30).

$$\begin{aligned} & \min_{\theta, \phi, \omega_y, \omega_s} \left[\mathcal{L}_{\text{VAE}}(\theta, \phi) + (\mathcal{L}_y(\omega_y, \phi) + \mathcal{L}_s(\omega_s, \phi)) \right] + \min_{\phi} \left[\right. \\ & \left. \lambda_{\text{CMI}} \mathcal{L}_{\text{CMI}}(\omega_{y_op}, \omega_{s_op}; \phi) + \mathcal{L}_{\text{TC}}(\phi) + \lambda_{\text{LRI}} \mathcal{L}_{\text{LRI}}(\omega_y, \omega_s; \phi) \right] \end{aligned} \quad (29)$$

Specifically, in (29), we jointly update $(\theta, \phi, \omega_y, \omega_s)$ by minimizing the VAE loss (5) alongside the main classification losses (8) and (9), which together reformulate the ELBO. We further include the CMI loss (20) to reduce unwanted information leakage, the LRI loss (22) to capture shared patterns in z_R , and the TC penalty (6) to promote factorization among the latent codes (z_Y, z_R, z_S) .

$$\min_{\omega_{y_op}, \omega_{s_op}} \left[\mathcal{L}_{y_op}(\omega_{y_op}; \phi) + \mathcal{L}_{s_op}(\omega_{s_op}; \phi) \right] \quad (30)$$

In parallel, the second procedure (30) optimizes $(\omega_{y_op}, \omega_{s_op})$ by minimizing the opponent classification losses (10) and (11) while holding ϕ fixed.

The hyperparameters $\lambda_{\text{CMI}}, \lambda_{\text{LRI}} > 0$ control the relative importance of these terms, ensuring each network component learns its designated function while enforcing minimal information leakage, preserving shared information in z_R and maintaining the salient factors for Y and S in z_Y and z_S respectively. See hypermeter analysis in *Appendix 6*.

Experiment

To ensure a rigorous and comprehensive evaluation, we conduct experiments comparing our proposed method with a diverse set of state-of-the-art approaches across multiple categories of learning paradigms in various tasks. Specifically, we include FairFactorVAE (Liu, Sun, and Zhao 2023), FairDisCo (Liu et al. 2022), FFVAE (Creager et al. 2019), GVAE (Ding et al. 2020), ODVAE (Sarhan et al. 2020) and FADES (Jang and Wang 2024), shown in Section 2.1. As for traditional correlation-aware learning that is discussed in Section 2.2, since it require additional annotated data to build causal graph, we except them in our experiment.

Fair Classification

The objective of fair classification is to achieve a balance between minimizing fairness violations and maintaining high predictive performance. To evaluate the effectiveness of our proposed method, we conduct experiments on a diverse set of benchmark fairness datasets. For facial attribute classification tasks, we utilize the CelebA (Liu et al. 2015) and UTKFace

Table 2: **Fair Classification on 95% Color Bias MNIST**

Metric	Ours	FADES	GVAE	FFVAE	ODVAE	FairFactorVAE
Accuracy ↑	0.867	0.782	0.771	0.744	0.721	0.807
EOD ↓	0.141	0.174	0.244	0.190	0.210	0.195
DP ↓	0.167	0.201	0.265	0.213	0.262	0.221

(Zhang, Song, and Qi 2017) datasets. Following prior works (Wang et al. 2022; Xu et al. 2020; Zeng et al. 2022; Jang and Wang 2024), we set the CelebA classification task to predict the “Smiling” attribute, while for UTKFace, the objective is to classify whether a person depicted in the image is over 35 years old, with gender serving as the sensitive attribute. Additionally, the Dogs and Cats dataset (Parkhi et al. 2012) is used to distinguish between dogs and cats, with fur color as the sensitive attribute. Furthermore, we assess fair classification performance using the Colored MNIST dataset (Kim, Lee, and Choo 2021; Kim et al. 2019; Nam et al. 2020), which incorporates a controlled color bias in the standard MNIST dataset to simulate spurious correlations. To assess fairness violations, we use standard metrics including Demographic Parity (DP) (Barocas and Selbst 2016) and Equalized Odds (EOD) (Hardt, Price, and Srebro 2016). See detailed experimental setup in *Appendix 6*. The result of fair classification can be seen in Table 1. Across all evaluated datasets, our method consistently achieves state-of-the-art classification accuracy and fairness, validating its effectiveness in robust disentanglement by preserving high-quality target-related information while minimizing sensitive attribute leakage.

To assess the robustness and effectiveness of these methods, we further conduct classification experiments under an extreme imbalance bias setting, which is commonly encountered in practical applications. In the MNIST experiment, we set the color bias rate to 95% to simulate a strong correlation between the target attribute and the sensitive attribute. The results, shown in Table 2, demonstrate that our method outperforms existing approaches in both disentanglement ability and robust representation preservation.

Fair Counterfactual Generation

We evaluate our approach on the CelebA dataset (Liu et al. 2015), a widely-used benchmark for facial attribute manipulation. We select *Smiling* as the target label Y and *Gender* as the sensitive attribute S . In our experiments, we substitute specific latent code of source images with reference images, including z_X , z_Y , z_S , and $[z_S, z_R]$. Figure 2 illustrates the generated counterfactuals, with the first row showing source and reference images and subsequent rows demonstrating the effects of substituting each latent code. The experimental results demonstrate the effectiveness of our method in generating fair counterfactuals. As shown in Figure 2, substituting

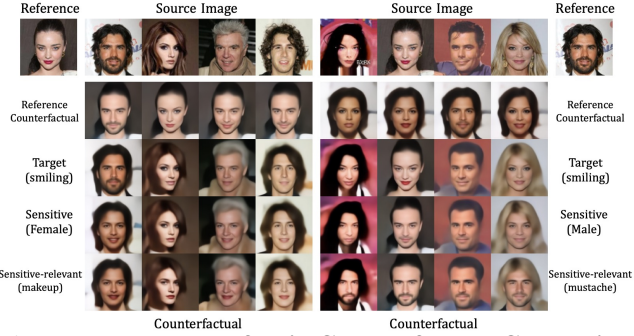


Figure 2: **Examples of Fair Counterfactual Generation.** Zoom in to check. The first row shows the source and reference images. Rows 2–5 display counterfactuals obtained by replacing latent subspaces z_X , z_Y , z_S , and $[z_S, z_R]$, respectively. Notably, the replacement with $[z_S, z_R]$ (row 5) naturally adapts sensitive features for different sensitive attributes without domain knowledge. (mustache for men and makeup for women).

$[z_S, z_R]$ (Row 5) leads to a natural adaptation of sensitive-relevant features without domain-specific knowledge. For instance, the model automatically adds makeup to female images and a mustache to male images, highlighting the semantic alignment of z_R with both the target and sensitive attributes. Compared to substituting only z_S , our approach achieves more interpretable translation, ensuring that fairness is maintained throughout the counterfactual generation. More fair counterfactual generation experiment results can be seen in *Appendix 7*.

To quantitatively assess the quality of the generated counterfactuals, we compare evaluation metrics between the direct reconstruction of the input image and the reconstructions obtained by randomly permuting z_Y and z_S within the evaluation set. Specifically, we use the FID (Heusel et al. 2017; Jang and Wang 2024) to assess reconstruction fidelity and the Inception Score (IS) (Chong and Forsyth 2020) to evaluate semantic and perceptual quality. Lower Δ FID values indicate minimal distortion and higher translation quality, while lower Δ IS values suggest that semantic and perceptual attributes are well preserved. Detailed experimental settings are provided in *Appendix 6*.

Table 3: **FID and IS difference between original reconstruction and perturbed target/sensitive codes’ reconstruction.**

	CAD-VAE	FADES	GVAE	FFVAE	ODVAE	FairFactorVAE
Δ FID ↓	1.072	1.167	3.710	1.409	14.647	6.239
Δ IS ↓	1.214	2.379	3.148	3.829	6.113	5.378

Quantitative analysis in Table 3 further validates our approach. Our method achieves both lower Δ FID and Δ IS compared to other fair representation learning methods, demonstrating that our fair counterfactual generation approach renders counterfactuals with superior image quality and minimal distortion.

Fair Fine-Grained Image Editing

With the introduction of the correlated latent code z_R , fair fine-grained image editing—as a fundamental concept in

counterfactual fairness—can be naturally achieved by aligning latent codes from different samples. We use linear interpolation to synthesize a latent code: $z' = (1 - \lambda)z_1 + \lambda z_2$, where z_1 is the latent code from the source image and z_2 is the corresponding code from the reference image. The synthesized z' replaces z_1 , enabling a gradual transfer from the source to the reference latent code.

In our experiments, following the setup in the previous section where *Smiling* is the target label Y and *Gender* is the sensitive attribute S , we generate interpolated latent codes between source and reference images. In the blue-framed subfigure of Figure 6, images are generated by interpolating z_Y and z_S : the horizontal axis shows the transition of z_S from the source to the reference image, while the vertical axis shows the corresponding change in z_Y . During this interpolation, z_R and z_X remain unchanged, with the interpolation parameters for both z_Y and z_S set to $\lambda \in \{0, 0.33, 0.66, 1\}$.

Similarly, in the red-framed subfigure, images are generated by interpolating z_Y and z_R . Here, the horizontal axis corresponds to the transition of z_R from the source to the reference image, and the vertical axis corresponds to z_Y . Note that the source image’s z_S is fully replaced by that of the reference image, and z_X remains constant. Initially, the interpolation parameters for z_R are set to $\lambda \in \{0.5, 1\}$, and when combined with the final column of the blue-framed subfigure, the range is extended to $\lambda \in \{0, 0.5, 1\}$.

Figure 6 demonstrates a smooth transformation of each attribute, with modifications in one latent code minimally affecting the others, a key characteristic of effective disentanglement. Specifically, as the correlated latent code z_R captures sensitive relevant information, we can explicitly control these properties: in the left subfigure, we gradually introduce makeup (such as enhanced lipstick and eyeshadow), while in the right subfigure, we progressively add a mustache. More fair fine-grained image editing experiment results can be seen in *Appendix 7*.

Similarly, we measure Δ FID and Δ IS to quantitatively assess the quality of fine-grained image editing. Unlike the evaluation setup in the previous section, we compute the differences in evaluation metrics between the direct reconstruction of the input image and the reconstructions obtained through latent code traversals for each λ combination. Detailed experimental settings are provided in *Appendix 6*. Table 4 summarizes the comparison results, showing that our method exhibits both lower Δ FID and Δ IS values compared to other fair generation methods. These results indicate that our fine-grained image editing approach not only ensures smoother attribute transformations and superior image fidelity, but also allows for more precise control of task-relevant features.

Fair Text-to-Image Editing

To further validate the capability and explore the applicability of our method, we integrated it as an adaptor on top of a pre-trained, frozen CLIP image encoder (Radford et al. 2021; Xiao et al. 2025c,a,b) and trained it on Facet dataset (Gustafson et al. 2023) to enhance fairness in vision-language tasks. Table 5 presents the experimental results. These results demonstrate that our approach significantly improves fairness without compromising performance com-

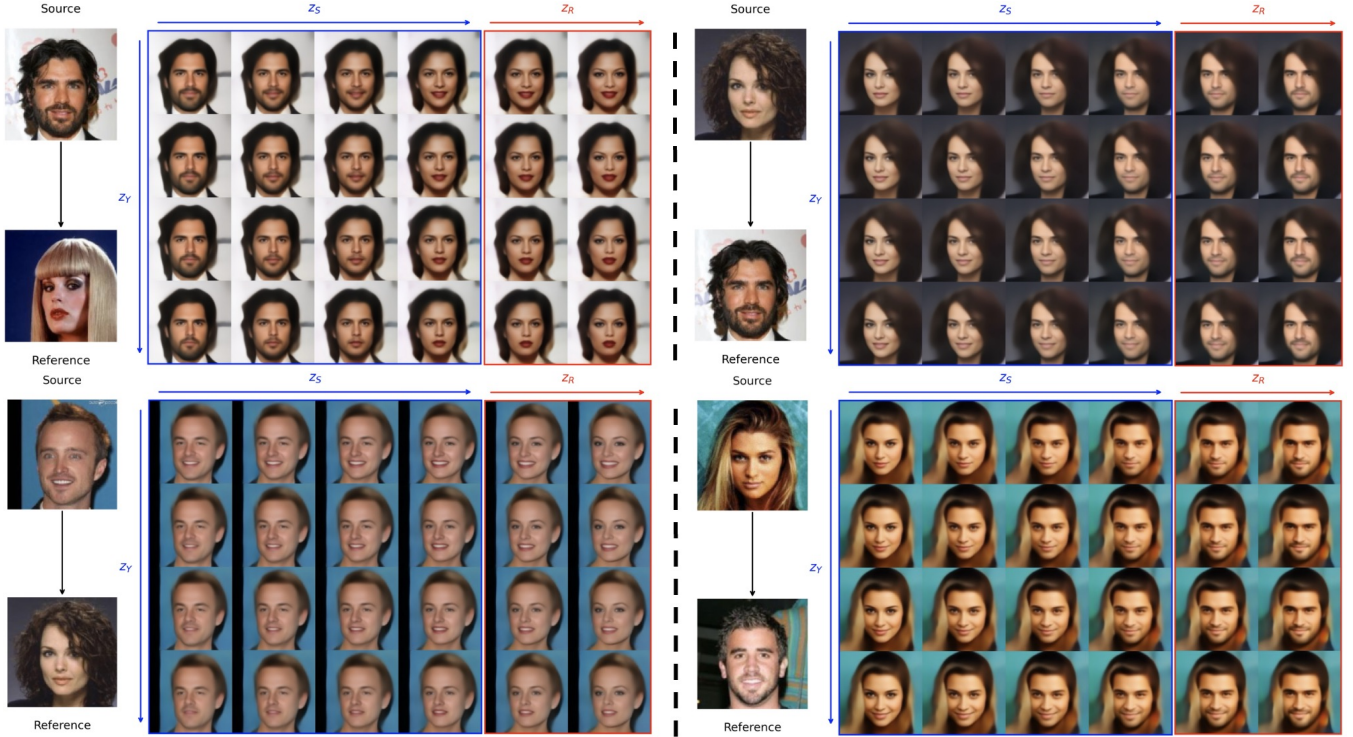


Figure 3: Examples of Fair Fine-Grained Image Editing. Zoom in to check. The leftmost column shows the source and reference images. The blue-framed section displays images generated by interpolating z_Y and z_S (with z_R and z_X fixed), where the horizontal axis varies z_S and the vertical axis varies z_Y . The red-framed section illustrates images produced by interpolating z_Y and z_R (with z_S fully replaced by the reference and z_X constant). Modification in one latent code minimally affecting others, harness z_R to edit sensitive relevant feature(makeup or mustache).

pared to the linear probing baseline (ERM), underscoring its potential for a range of vision-language tasks with fairness considerations.

Furthermore, we applied our method in StyleCLIP (Patashnik et al. 2021) as a fair discriminator to address inherent fairness issues, such as career-gender biases, which persist even when an identity preservation loss is employed. As illustrated in Figure 8, StyleCLIP (Patashnik et al. 2021) exhibits a bias by correlating the role of “dancer” with a specific gender. In contrast, our method effectively mitigates this bias while maintaining the efficacy of attribute modification. See Appendix 7 for details.

Table 4: FID and IS difference between original reconstruction and traversed target/sensitive codes’ reconstruction.

	CAD-VAE	FADES	GVAE	FFVAE	ODVAE	FairFactorVAE
$\Delta FID \downarrow$	1.642	2.362	4.023	2.789	15.893	7.120
$\Delta IS \downarrow$	1.849	2.919	4.848	5.292	6.890	5.767

Table 5: Performance of CLIP(ViT/32) on Facet dataset. WG: Worst Group, Gap: Difference between WG and Avg.

Method	Top-1 Acc. (%)			Top-3 Acc. (%)		
	WG \uparrow	Avg \uparrow	Gap \downarrow	WG \uparrow	Avg \uparrow	Gap \downarrow
Zero-shot	2.79	53.45	50.66	15.31	76.79	61.48
Linear prob	1.17	65.46	64.29	1.79	85.34	83.55
CAD-VAE	69.97	70.54	0.57	85.36	85.95	0.59



Figure 4: Style transfer using StyleCLIP and the CAD-VAE extension. This example transforms the (a) into “a dancer with long blonde hair.” “StyleCLIP+” means StyleCLIP + CAD-VAE.

Conclusion

Our method aims to solve fairness concerns in representation learning and deep generative models. By introducing a correlated latent code that captures shared information, sensitive information leakage can be eliminated directly and efficiently without conflicting with the prediction objective, which is a core issue in disentanglement, by minimizing the conditional mutual information between target latent code and sensitive latent code. Parallel with our explicit relevance learning strategy imposed on the correlated latent code, it is encouraged to capture the essential shared information that cannot be perfectly separated without additional domain knowledge. Various benchmark tasks further demonstrate the robustness and wide applicability of our method.

Acknowledgment

This manuscript was co-authored by Oak Ridge National Laboratory (ORNL), operated by UT-Battelle, LLC under Contract No. DE-AC05-00OR22725 with the U.S. Department of Energy. Any subjective views or opinions expressed in this paper do not necessarily represent those of the U.S. Department of Energy or the United States Government.

References

Bai, J.; Ye, T.; Chow, W.; Song, E.; Chen, Q.-G.; Li, X.; Dong, Z.; Zhu, L.; and Shuicheng, Y. 2024. Meissonic: Revitalizing masked generative transformers for efficient high-resolution text-to-image synthesis. In *The Thirteenth International Conference on Learning Representations*.

Barocas, S.; and Selbst, A. D. 2016. Big data’s disparate impact. *Calif. L. Rev.*, 104: 671.

Chen, R. T.; Li, X.; Grosse, R. B.; and Duvenaud, D. K. 2018. Isolating sources of disentanglement in variational autoencoders. *Advances in neural information processing systems*, 31.

Chiappa, S. 2019. Path-specific counterfactual fairness. In *Proceedings of the AAAI conference on artificial intelligence*, volume 33, 7801–7808.

Chong, M. J.; and Forsyth, D. 2020. Effectively unbiased fid and inception score and where to find them. In *Proceedings of the IEEE/CVF conference on computer vision and pattern recognition*, 6070–6079.

Creager, E.; Madras, D.; Jacobsen, J.-H.; Weis, M.; Swersky, K.; Pitassi, T.; and Zemel, R. 2019. Flexibly fair representation learning by disentanglement. In *International conference on machine learning*, 1436–1445. PMLR.

Ding, Z.; Xu, Y.; Xu, W.; Parmar, G.; Yang, Y.; Welling, M.; and Tu, Z. 2020. Guided variational autoencoder for disentanglement learning. In *Proceedings of the IEEE/CVF conference on computer vision and pattern recognition*, 7920–7929.

Dressel, J.; and Farid, H. 2018. The accuracy, fairness, and limits of predicting recidivism. *Science Advances*, 4(1): eaao5580.

Gustafson, L.; Rolland, C.; Ravi, N.; Duval, Q.; Adcock, A.; Fu, C.-Y.; Hall, M.; and Ross, C. 2023. FACET: Fairness in Computer Vision Evaluation Benchmark. arXiv:2309.00035.

Hardt, M.; Price, E.; and Srebro, N. 2016. Equality of opportunity in supervised learning. *Advances in neural information processing systems*, 29.

He, K.; Zhang, X.; Ren, S.; and Sun, J. 2016. Deep residual learning for image recognition. In *Proceedings of the IEEE conference on computer vision and pattern recognition*, 770–778.

Heusel, M.; Ramsauer, H.; Unterthiner, T.; Nessler, B.; and Hochreiter, S. 2017. Gans trained by a two time-scale update rule converge to a local nash equilibrium. *Advances in neural information processing systems*, 30.

Higgins, I.; Matthey, L.; Pal, A.; Burgess, C.; Glorot, X.; Botvinick, M.; Mohamed, S.; and Lerchner, A. 2017. betavae: Learning basic visual concepts with a constrained variational framework. In *International conference on learning representations*.

Hwa, J.; Zhao, Q.; Lahiri, A.; Masood, A.; Salimi, B.; and Adeli, E. 2024. Enforcing Conditional Independence for Fair Representation Learning and Causal Image Generation. In *Proceedings of the IEEE/CVF Conference on Computer Vision and Pattern Recognition*, 103–112.

Jang, T.; and Wang, X. 2024. FADES: Fair Disentanglement with Sensitive Relevance. In *Proceedings of the IEEE/CVF Conference on Computer Vision and Pattern Recognition (CVPR)*, 12067–12076.

Jung, S.; Yu, S.; Chun, S.; and Moon, T. 2025. Do Counterfactually Fair Image Classifiers Satisfy Group Fairness?—A Theoretical and Empirical Study. *Advances in Neural Information Processing Systems*, 37: 56041–56053.

Kim, B.; Kim, H.; Kim, K.; Kim, S.; and Kim, J. 2019. Learning Not to Learn: Training Deep Neural Networks With Biased Data. In *Proceedings of the IEEE/CVF Conference on Computer Vision and Pattern Recognition (CVPR)*.

Kim, E.; Lee, J.; and Choo, J. 2021. Biaswap: Removing dataset bias with bias-tailored swapping augmentation. In *Proceedings of the IEEE/CVF International Conference on Computer Vision*, 14992–15001.

Kim, H.; and Mnih, A. 2018. Disentangling by factorising. In *International conference on machine learning*, 2649–2658. PMLR.

Kim, H.; Shin, S.; Jang, J.; Song, K.; Joo, W.; Kang, W.; and Moon, I.-C. 2021. Counterfactual fairness with disentangled causal effect variational autoencoder. In *Proceedings of the AAAI Conference on Artificial Intelligence*, volume 35, 8128–8136.

Kingma, D. P.; and Welling, M. 2022. Auto-Encoding Variational Bayes. arXiv:1312.6114.

Kohavi, R. 1996. Scaling up the accuracy of Naive-Bayes classifiers: a decision-tree hybrid. In *Proceedings of the Second International Conference on Knowledge Discovery and Data Mining*, KDD’96, 202–207. AAAI Press.

Kusner, M. J.; Loftus, J.; Russell, C.; and Silva, R. 2017. Counterfactual fairness. *Advances in neural information processing systems*, 30.

Lahoti, P.; Beutel, A.; Chen, J.; Lee, K.; Prost, F.; Thain, N.; Wang, X.; and Chi, E. H. 2020. Fairness without Demographics through Adversarially Reweighted Learning. arXiv:2006.13114.

Li, H.; Liu, Y.; Geng, Z.; and Zhang, K. 2025. A Local Method for Satisfying Interventional Fairness with Partially Known Causal Graphs. *Advances in Neural Information Processing Systems*, 37: 135415–135436.

Liu, E. Z.; Haghgoo, B.; Chen, A. S.; Raghunathan, A.; Koh, P. W.; Sagawa, S.; Liang, P.; and Finn, C. 2021. Just Train Twice: Improving Group Robustness without Training Group Information. arXiv:2107.09044.

Liu, J.; Li, Z.; Yao, Y.; Xu, F.; Ma, X.; Xu, M.; and Tong, H. 2022. Fair representation learning: An alternative to mutual information. In *Proceedings of the 28th ACM SIGKDD Conference on Knowledge Discovery and Data Mining*, 1088–1097.

Liu, S.; Sun, S.; and Zhao, J. 2023. Fair transfer learning with factor variational auto-encoder. *Neural Processing Letters*, 55(3): 2049–2061.

Liu, Z.; Luo, P.; Wang, X.; and Tang, X. 2015. Deep learning face attributes in the wild. In *Proceedings of the IEEE international conference on computer vision*, 3730–3738.

Ma, C.; Xiao, X.; Wang, T.; and Shen, Y. 2025a. Beyond Editing Pairs: Fine-Grained Instructional Image Editing via Multi-Scale Learnable Regions. *arXiv preprint arXiv:2505.19352*.

Ma, C.; Xiao, X.; Wang, T.; Wang, X.; and Shen, Y. 2025b. Learning Straight Flows: Variational Flow Matching for Efficient Generation. *arXiv preprint*.

Ma, C.; Xiao, X.; Wang, T.; Wang, X.; and Shen, Y. 2025c. Stochastic Interpolants via Conditional Dependent Coupling. *arXiv preprint arXiv:2509.23122*.

Madras, D.; Creager, E.; Pitassi, T.; and Zemel, R. 2018. Learning adversarially fair and transferable representations. In *International Conference on Machine Learning*, 3384–3393. PMLR.

Mathieu, E.; Rainforth, T.; Siddharth, N.; and Teh, Y. W. 2019. Disentangling Disentanglement in Variational Autoencoders. *arXiv:1812.02833*.

Mehrabi, N.; Morstatter, F.; Saxena, N.; Lerman, K.; and Galstyan, A. 2021. A survey on bias and fairness in machine learning. *ACM computing surveys (CSUR)*, 54(6): 1–35.

Montanaro, A.; Aira, L. S.; Aiello, E.; Valsesia, D.; and Magli, E. 2024. MotionCraft: Physics-Based Zero-Shot Video Generation. In Globersons, A.; Mackey, L.; Belgrave, D.; Fan, A.; Paquet, U.; Tomczak, J. M.; and Zhang, C., eds., *Advances in Neural Information Processing Systems 38: Annual Conference on Neural Information Processing Systems 2024, NeurIPS 2024, Vancouver, BC, Canada, December 10 - 15, 2024*.

Nam, J.; Cha, H.; Ahn, S.; Lee, J.; and Shin, J. 2020. Learning from failure: De-biasing classifier from biased classifier. *Advances in Neural Information Processing Systems*, 33: 20673–20684.

Park, S.; Kim, D.; Hwang, S.; and Byun, H. 2020. README: REpresentation learning by fairness-Aware Disentangling MEthod. *arXiv:2007.03775*.

Parkhi, O. M.; Vedaldi, A.; Zisserman, A.; and Jawahar, C. 2012. Cats and dogs. In *2012 IEEE conference on computer vision and pattern recognition*, 3498–3505. IEEE.

Patashnik, O.; Wu, Z.; Shechtman, E.; Cohen-Or, D.; and Lischinski, D. 2021. StyleCLIP: Text-Driven Manipulation of StyleGAN Imagery. In *Proceedings of the IEEE/CVF International Conference on Computer Vision (ICCV)*, 2085–2094.

Radford, A.; Kim, J. W.; Hallacy, C.; Ramesh, A.; Goh, G.; Agarwal, S.; Sastray, G.; Askell, A.; Mishkin, P.; Clark, J.; Krueger, G.; and Sutskever, I. 2021. Learning Transferable Visual Models From Natural Language Supervision. *arXiv:2103.00020*.

Roy, P. C.; and Boddeti, V. N. 2019. Mitigating Information Leakage in Image Representations: A Maximum Entropy Approach. *arXiv:1904.05514*.

Sánchez-Martin, P.; Rateike, M.; and Valera, I. 2022. Vaca: Designing variational graph autoencoders for causal queries. In *Proceedings of the AAAI Conference on Artificial Intelligence*, volume 36, 8159–8168.

Sarhan, M. H.; Navab, N.; Eslami, A.; and Albarqouni, S. 2020. Fairness by learning orthogonal disentangled representations. In *Computer Vision–ECCV 2020: 16th European Conference, Glasgow, UK, August 23–28, 2020, Proceedings, Part XXIX 16*, 746–761. Springer.

Wang, X.; Chen, H.; Tang, S.; Wu, Z.; and Zhu, W. 2024. Disentangled Representation Learning. *IEEE Transactions on Pattern Analysis and Machine Intelligence*, 46(12): 9677–9696.

Wang, Z.; Dong, X.; Xue, H.; Zhang, Z.; Chiu, W.; Wei, T.; and Ren, K. 2022. Fairness-aware adversarial perturbation towards bias mitigation for deployed deep models. In *Proceedings of the IEEE/CVF conference on computer vision and pattern recognition*, 10379–10388.

Wu, Y.; Zhang, L.; and Wu, X. 2019. Counterfactual fairness: Unidentification, bound and algorithm. In *Proceedings of the twenty-eighth international joint conference on Artificial Intelligence*.

Xiao, X.; Zhang, Y.; Li, X.; Wang, T.; Wang, X.; Wei, Y.; Hamm, J.; and Xu, M. 2025a. Visual Instance-aware Prompt Tuning. In *Proceedings of the 33rd ACM International Conference on Multimedia*.

Xiao, X.; Zhang, Y.; Li, Y.; Li, X.; Wang, T.; Hamm, J.; Wang, X.; and Xu, M. 2025b. Visual Variational Autoencoder Prompt Tuning. *arXiv preprint arXiv:2503.17650*.

Xiao, X.; Zhang, Y.; Zhao, L.; Liu, Y.; Liao, X.; Mai, Z.; Li, X.; Wang, X.; Xu, H.; Hamm, J.; et al. 2025c. Prompt-based Adaptation in Large-scale Vision Models: A Survey. *arXiv preprint arXiv:2510.13219*.

Xu, D.; Yuan, S.; Zhang, L.; and Wu, X. 2018. Fairgan: Fairness-aware generative adversarial networks. In *2018 IEEE international conference on big data (big data)*, 570–575. IEEE.

Xu, T.; White, J.; Kalkan, S.; and Gunes, H. 2020. Investigating bias and fairness in facial expression recognition. In *Computer Vision–ECCV 2020 Workshops: Glasgow, UK, August 23–28, 2020, Proceedings, Part VI 16*, 506–523. Springer.

Zeng, H.; Yue, Z.; Shang, L.; Zhang, Y.; and Wang, D. 2022. Boosting demographic fairness of face attribute classifiers via latent adversarial representations. In *2022 IEEE International Conference on Big Data (Big Data)*, 1588–1593. IEEE.

Zhang, Z.; Song, Y.; and Qi, H. 2017. Age progression/regression by conditional adversarial autoencoder. In *Proceedings of the IEEE conference on computer vision and pattern recognition*, 5810–5818.

Zhou, Z.; Liu, T.; Bai, R.; Gao, J.; Kocaoglu, M.; and Inouye, D. I. 2024. Counterfactual Fairness by Combining Factual and Counterfactual Predictions. *arXiv preprint arXiv:2409.01977*.

Zhu, H.; Dai, E.; Liu, H.; and Wang, S. 2023. Learning fair models without sensitive attributes: A generative approach. *Neurocomputing*, 561: 126841.

Appendix

Relation between Conditional Mutual Information and Conditional Independence

Proposition 2. Let X, Y, Z be random variables with a joint distribution $P_{X,Y,Z}$. Then the following are equivalent:

1. $I(X; Y | Z) = 0$,
2. X and Y are conditionally independent given Z , i.e., $X \perp Y | Z$.

(2) \implies (1). If X is conditionally independent of Y given Z , we have

$$P_{X,Y|Z}(x, y | z) = P_{X|Z}(x | z) P_{Y|Z}(y | z). \quad (31)$$

Thus, for each z with $P_Z(z) > 0$,

$$\log \left[\frac{P_{X,Y|Z}(x, y | z)}{P_{X|Z}(x | z) P_{Y|Z}(y | z)} \right] = \log(1) = 0. \quad (32)$$

Therefore,

$$I(X; Y | Z)$$

$$\begin{aligned} &= \sum_z P_Z(z) \sum_{x,y} P_{X,Y|Z}(x, y | z) \log \left[\frac{P_{X,Y|Z}(x, y | z)}{P_{X|Z}(x | z) P_{Y|Z}(y | z)} \right] \\ &= 0. \end{aligned} \quad (33)$$

(1) \implies (2). Suppose $I(X; Y | Z) = 0$. Define

$$F(x, y) := \frac{P_{X|Z}(x | z) P_{Y|Z}(y | z)}{P_{X,Y|Z}(x, y | z)}, \quad (34)$$

for each z such that $P_Z(z) > 0$. A direct calculation shows

$$\begin{aligned} &\sum_{x,y} P_{X,Y|Z}(x, y | z) F(x, y) \\ &= \sum_{x,y} P_{X|Z}(x | z) P_{Y|Z}(y | z) = 1. \end{aligned} \quad (35)$$

The conditional mutual information can be written as

$$I(X; Y | Z)$$

$$\begin{aligned} &= \sum_z P_Z(z) \sum_{x,y} P_{X,Y|Z}(x, y | z) \log \left[\frac{P_{X,Y|Z}(x, y | z)}{P_{X|Z}(x | z) P_{Y|Z}(y | z)} \right] \\ &= - \sum_z P_Z(z) \sum_{x,y} P_{X,Y|Z}(x, y | z) \log F(x, y). \end{aligned} \quad (36)$$

Using the identity

$$-\log F(x, y) = [F(x, y) - 1 - \log F(x, y)] - [F(x, y) - 1], \quad (37)$$

and rearranging, one obtains

$$\begin{aligned} &I(X; Y | Z) \\ &= \sum_z P_Z(z) \sum_{x,y} P_{X,Y|Z}(x, y | z) [F(x, y) - 1 - \log F(x, y)]. \end{aligned} \quad (38)$$

To see why this rearrangement holds, substitute the above identity into $\sum_{x,y} P_{X,Y|Z}(x, y | z) \log F(x, y)$. The

result is a difference of two sums; one of these sums, $\sum_{x,y} P_{X,Y|Z}(x, y | z) [F(x, y) - 1]$, is zero because

$$\begin{aligned} &\sum_{x,y} P_{X,Y|Z}(x, y | z) [F(x, y) - 1] \\ &= \sum_{x,y} P_{X,Y|Z}(x, y | z) F(x, y) - \sum_{x,y} P_{X,Y|Z}(x, y | z) \\ &= 1 - 1 = 0. \end{aligned} \quad (39)$$

Hence we arrive at the above expression for (38). Since $\log t \leq t - 1$ for all $t > 0$, we have

$$F(x, y) - 1 - \log F(x, y) \geq 0, \quad (40)$$

and hence each summand in the expression for $I(X; Y | Z)$ is nonnegative. Because $I(X; Y | Z) = 0$ by hypothesis, it must be that

$$F(x, y) - 1 - \log F(x, y) = 0 \quad \text{for all } x, y, \quad (41)$$

implying $F(x, y) = 1$. Therefore,

$$F(x, y) = \frac{P_{X|Z}(x | z) P_{Y|Z}(y | z)}{P_{X,Y|Z}(x, y | z)} = 1, \quad (42)$$

so that

$$P_{X,Y|Z}(x, y | z) = P_{X|Z}(x | z) P_{Y|Z}(y | z). \quad (43)$$

This is precisely the definition of conditional independence: $X \perp Y | Z$.

Since we have shown both directions (2) \implies (1) and (1) \implies (2), the proof is complete.

Complete Transformation Process of Conditional Mutual Information

$H_\phi(\cdot | \cdot)$ stand the conditional entropy, and

$$\hat{Y} = f_y(z_Y, z_R) \quad (44)$$

$$\hat{S} = f_s(z_S, z_R). \quad (45)$$

Incorporating (45), we have:

$$\begin{aligned} I_\phi(\hat{Y}; \hat{S} | z_R) &= H_\phi(\hat{Y} | z_R) - H_\phi(\hat{Y} | \hat{S}, z_R) \\ &= H_\phi(\hat{Y} | z_R) - H_\phi(\hat{Y} | f_s(z_S, z_R), z_R) \\ &= H_\phi(\hat{Y} | z_R) - H_\phi(\hat{Y} | z_S, z_R) \\ &= I_\phi(\hat{Y}; z_S | z_R). \end{aligned} \quad (46)$$

Incorporating (44), we have:

$$\begin{aligned} I_\phi(\hat{S}; \hat{Y} | z_R) &= H_\phi(\hat{S} | z_R) - H_\phi(\hat{S} | \hat{Y}, z_R) \\ &= H_\phi(\hat{S} | z_R) - H_\phi(\hat{S} | f_y(z_Y, z_R), z_R) \\ &= H_\phi(\hat{S} | z_R) - H_\phi(\hat{S} | z_Y, z_R) \\ &= I_\phi(\hat{S}; z_Y | z_R). \end{aligned} \quad (47)$$

Therefore, with the introduction of the correlated latent code z_R that captures all relevant information between \hat{Y} and \hat{S} :

$$\begin{aligned} \min_{\phi} & \left[I_{\phi}(\hat{Y}; \hat{S} | z_R) + I_{\phi}(\hat{S}; \hat{Y} | z_R) \right] \\ & \equiv \min_{\phi} \left[I_{\phi}(\hat{Y}; z_S | z_R) + I_{\phi}(\hat{S}; z_Y | z_R) \right]. \end{aligned} \quad (48)$$

For the minimization of $I_{\phi}(\hat{Y}; z_S | z_R)$, as shown in (46), since z_R is given as a condition, we can consider this CMI formula as a function where the independent variable is z_S and the dependent variable is \hat{Y} , as shown as:

$$\mathcal{L}_{\hat{Y}}(z_S) = H_{\phi}(\hat{Y} | z_R) - H_{\phi}(\hat{Y} | z_S, z_R), \quad (49)$$

where z_R is determined here, $H_{\phi}(\hat{Y} | z_R)$ is a constant, henceforth we need to minimize $-H_{\phi}(\hat{Y} | z_S, z_R)$. Empirically, we directly minimize the lower bound of it: $-H_{\phi}(\hat{Y} | z_S)$, since: $-H_{\phi}(\hat{Y} | z_S, z_R) \geq -H_{\phi}(\hat{Y} | z_S)$.

For the minimization of $I_{\phi}(\hat{S}; z_Y | z_R)$, as shown in (47), since z_R is given as a condition, we can consider this CMI formula as a function where the independent variable is z_Y and the dependent variable is \hat{S} , as shown as:

$$\mathcal{L}_{\hat{S}}(z_Y) = H_{\phi}(\hat{S} | z_R) - H_{\phi}(\hat{S} | z_Y, z_R), \quad (50)$$

where z_R is determined here, $H_{\phi}(\hat{S} | z_R)$ is a constant, henceforth we need to minimize $-H_{\phi}(\hat{S} | z_Y, z_R)$. Empirically, we directly minimize the lower bound of it: $-H_{\phi}(\hat{S} | z_Y)$, since: $-H_{\phi}(\hat{S} | z_Y, z_R) \geq -H_{\phi}(\hat{S} | z_Y)$.

After these simplifications, we can introduce the CMI loss to minimize (48):

$$\min_{\phi} \left[\mathcal{L}_{\text{CMI}}(\omega_{y_op}; \omega_{s_op}; \phi) \right] = -(H_{\phi}(\hat{Y} | z_S) + H_{\phi}(\hat{S} | z_Y)), \quad (51)$$

where only update encoder parameters ϕ .

Complete Calculation Formula of Entropy Term mentioned in Main Paper

1. $H_{\phi}(\hat{Y} | z_S)$: We use the opponent classifier $f_{y_op}(z_S)$, which predicts y from z_S . Denoting

$$p_{\theta}(\hat{y} | z_S^{(k)}) = f_{y_op}(z_S^{(k)}),$$

then

$$\begin{aligned} H_{\phi}(\hat{Y} | z_S) &= \mathbb{E}_{q_{\phi}(z_S | x)} \left[- \sum_{\hat{y} \in \mathcal{Y}} p_{\theta}(\hat{y} | z_S) \log p_{\theta}(\hat{y} | z_S) \right] \\ &= \frac{1}{|B|} \sum_{i=1}^{|B|} \sum_{\hat{y} \in \mathcal{Y}} \left[-p_{\theta}(\hat{y} | z_S^{(i)}) \log p_{\theta}(\hat{y} | z_S^{(i)}) \right]. \end{aligned} \quad (52)$$

Here, $z_S^{(i)}$ denotes the z_S sample from the i -th element in a mini-batch of size $|B|$; the distribution $q_{\phi}(z_S | x)$ is given by the encoder.

2. $H_{\phi}(\hat{S} | z_Y)$: Similarly, we employ the opponent classifier $f_{s_op}(z_Y)$ to measure how much z_Y retains information about s . We define

$$p_{\theta}(\hat{s} | z_Y^{(k)}) = f_{s_op}(z_Y^{(k)}),$$

and

$$\begin{aligned} H_{\phi}(\hat{S} | z_Y) &= \mathbb{E}_{q_{\phi}(z_Y | x)} \left[- \sum_{\hat{s} \in \mathcal{S}} p_{\theta}(\hat{s} | z_Y) \log p_{\theta}(\hat{s} | z_Y) \right] \\ &= \frac{1}{|B|} \sum_{i=1}^{|B|} \sum_{\hat{s} \in \mathcal{S}} \left[-p_{\theta}(\hat{s} | z_Y^{(i)}) \log p_{\theta}(\hat{s} | z_Y^{(i)}) \right]. \end{aligned} \quad (53)$$

Here, $z_Y^{(i)}$ denotes the z_Y sample from the i -th element in a mini-batch of size $|B|$; the distribution $q_{\phi}(z_Y | x)$ is given by the encoder.

3. $H_{\phi}(\hat{Y} | z_R)$: We approximate $p_{\theta}(\hat{y} | z_R)$ by marginalizing over z_Y :

$$\begin{aligned} p_{\theta}(\hat{y} | z_R^{(k)}) &= \mathbb{E}_{p(x)} \left[\mathbb{E}_{q_{\phi}(z_Y | x)} \left[p_{\theta}(\hat{y} | z_Y, z_R^{(k)}) \right] \right] \\ &\approx \frac{1}{|B|} \sum_{i=1}^{|B|} p_{\theta}(\hat{y} | z_Y^{(i)}, z_R^{(k)}), \end{aligned} \quad (54)$$

where $p_{\theta}(\hat{y} | z_Y^{(i)}, z_R^{(k)})$ is obtained by $f_y(z_Y, z_R)$:

$$p_{\theta}(\hat{y} | z_Y^{(i)}, z_R^{(k)}) = f_y(z_Y^{(i)}, z_R^{(k)}), \quad (55)$$

then

$$\begin{aligned} H_{\phi}(\hat{Y} | z_R) &= \mathbb{E}_{q_{\phi}(z_R | x)} \left[- \sum_{\hat{y} \in \mathcal{Y}} p_{\theta}(\hat{y} | z_R) \log p_{\theta}(\hat{y} | z_R) \right] \\ &= \frac{1}{|B|} \sum_{i=1}^{|B|} \sum_{\hat{y} \in \mathcal{Y}} \left[-p_{\theta}(\hat{y} | z_R^{(i)}) \log p_{\theta}(\hat{y} | z_R^{(i)}) \right], \end{aligned} \quad (56)$$

4. $H_{\phi}(\hat{S} | z_R)$: We approximate $p_{\theta}(\hat{s} | z_R)$ by marginalizing over z_S :

$$\begin{aligned} p_{\theta}(\hat{s} | z_R^{(k)}) &= \mathbb{E}_{p(x)} \left[\mathbb{E}_{q_{\phi}(z_S | x)} \left[p_{\theta}(\hat{s} | z_S, z_R^{(k)}) \right] \right] \\ &\approx \frac{1}{|B|} \sum_{i=1}^{|B|} p_{\theta}(\hat{s} | z_S^{(i)}, z_R^{(k)}), \end{aligned} \quad (57)$$

where $p_{\theta}(\hat{s} | z_S^{(i)}, z_R^{(k)})$ is obtained by $f_s(z_S, z_R)$:

$$p_{\theta}(\hat{s} | z_S^{(i)}, z_R^{(k)}) = f_s(z_S^{(i)}, z_R^{(k)}), \quad (58)$$

then

$$\begin{aligned} H_{\phi}(\hat{S} | z_R) &= \mathbb{E}_{q_{\phi}(z_R | x)} \left[- \sum_{\hat{s} \in \mathcal{S}} p_{\theta}(\hat{s} | z_R) \log p_{\theta}(\hat{s} | z_R) \right] \\ &= \frac{1}{|B|} \sum_{i=1}^{|B|} \sum_{\hat{s} \in \mathcal{S}} \left[-p_{\theta}(\hat{s} | z_R^{(i)}) \log p_{\theta}(\hat{s} | z_R^{(i)}) \right], \end{aligned} \quad (59)$$

5. $H_\phi(\hat{Y} \mid Y, z_R)$: $p_\theta(\hat{y} \mid z_R, y)$ can be computed for $z_R^{(k)}$ sampled from an instance $x^{(k)} \in B_y$ as:

$$\begin{aligned} p_\theta(\hat{y} \mid z_R^{(k)}, y) &= \mathbb{E}_{p(x \mid Y=y)} \left[\mathbb{E}_{q_\phi(z_Y \mid x)} \left[p_\theta(\hat{y} \mid z_Y, z_R^{(k)}) \right] \right] \\ &\approx \frac{1}{|B_y|} \sum_{i=1}^{|B_y|} p_\theta(\hat{y} \mid z_Y^{(i)}, z_R^{(k)}), \end{aligned} \quad (60)$$

where B_y denotes a subset of the batch with $Y = y$. Then the conditional entropy can be computed as:

$$\begin{aligned} H_\phi(\hat{Y} \mid Y, z_R) &= \\ &\mathbb{E}_{(x,y) \sim \mathcal{D}} \left[\mathbb{E}_{q_\phi(z_R \mid x)} \left[-\sum_{\hat{y} \in \mathcal{Y}} p_\theta(\hat{y} \mid z_R, y) \log p_\theta(\hat{y} \mid z_R, y) \right] \right] \\ &= \frac{1}{|B|} \sum_{y \in \mathcal{Y}} \sum_{i=1}^{|B_y|} \sum_{\hat{y} \in \mathcal{Y}} \left[-p_\theta(\hat{y} \mid z_R^{(i)}, y) \log p_\theta(\hat{y} \mid z_R^{(i)}, y) \right]. \end{aligned} \quad (61)$$

6. $H_\phi(\hat{S} \mid S, z_R)$: $p_\theta(\hat{s} \mid z_R, s)$ can be computed for $z_R^{(k)}$ sampled from an instance $x^{(k)} \in B_s$ as:

$$\begin{aligned} p_\theta(\hat{s} \mid z_R^{(k)}, s) &= \mathbb{E}_{p(x \mid S=s)} \left[\mathbb{E}_{q_\phi(z_S \mid x)} \left[p_\theta(\hat{s} \mid z_S, z_R^{(k)}) \right] \right] \\ &\approx \frac{1}{|B_s|} \sum_{i=1}^{|B_s|} p_\theta(\hat{s} \mid z_S^{(i)}, z_R^{(k)}), \end{aligned} \quad (62)$$

where B_s denotes a subset of the batch with $S = s$. Then the conditional entropy can be computed as:

$$\begin{aligned} H_\phi(\hat{S} \mid S, z_R) &= \\ &\mathbb{E}_{(x,s) \sim \mathcal{D}} \left[\mathbb{E}_{q_\phi(z_R \mid x)} \left[-\sum_{\hat{s} \in \mathcal{S}} p_\theta(\hat{s} \mid z_R, s) \log p_\theta(\hat{s} \mid z_R, s) \right] \right] \\ &= \frac{1}{|B|} \sum_{s \in \mathcal{S}} \sum_{i=1}^{|B_s|} \sum_{\hat{s} \in \mathcal{S}} \left[-p_\theta(\hat{s} \mid z_R^{(i)}, s) \log p_\theta(\hat{s} \mid z_R^{(i)}, s) \right]. \end{aligned} \quad (63)$$

Experiment Setup Details

Comparison Methods

Specifically, we include FairFactorVAE (Kim and Mnih 2018) and FairDisCo (Liu et al. 2022), both of which leverage invariant learning techniques to encode latent representations that remain independent of sensitive attributes. Additionally, FFVAE (Creager et al. 2019) employs a mutual information minimization strategy to effectively disentangle latent subspaces. GVAE (Ding et al. 2020) takes a distinct approach by minimizing information leakage to achieve fair representation learning. ODVAE (Sarhan et al. 2020), in contrast, introduces a non-adversarial learning framework that enforces orthogonal priors on the latent subspace, promoting fairness without adversarial training. Finally, FADES (Jang and Wang 2024) proposes minimizing conditional mutual information to achieve fairness, aligning closely with our method. As

for traditional correlation-aware learning that discussed in Section 2.2, since it require additional annotated data to build causal graph, we except them in our experiment.

To ensure a fair comparison, we adopt a grid search strategy to fine-tune the hyperparameters of all methods, optimizing for Equalized Odds (EOD) (Hardt, Price, and Srebro 2016). Specifically, for our method, hyperparameters are explored within the ranges: $\lambda_{CMI} \in [0, 10]$ and $\lambda_{LRI} \in [0, 100]$. We maintain a consistent architectural setup across all methods, utilizing a ResNet-18 backbone (He et al. 2016) with 512 latent dimensions for all tasks.

Dimension of each latent code

In our experiment, we set equal dimensional sizes for $z_Y, z_S, z_R \in \mathbb{R}^d$, with d set as a power of 2. Through empirical selection via grid search, we determined $d = 32$ for the reported results. Notably, the total latent dimension was fixed at \mathbb{R}^{512} across all methods. Consequently, in our approach, we allocated $z_X \in \mathbb{R}^{512-3 \times 32} = \mathbb{R}^{416}$. Our empirical findings revealed that setting d beyond 64 led to a decline in reconstruction performance. This degradation likely stems from an excessive allocation of information to each subspace, ultimately compromising the model’s reconstructive capacity.

Hypermeter Analysis

We evaluated the effect of the two hyperparameters, $\lambda_{CMI} \in [0, 10]$ and $\lambda_{LRI} \in [0, 100]$, on both classification accuracy and fairness violation (measured as Equalized Odds Difference, EOD) in the CelebA dataset classification task. For the analysis of λ_{CMI} , we fixed λ_{LRI} at 60, while for the analysis of λ_{LRI} , we fixed λ_{CMI} at 5. The result can be seen in Figure 5.

Specifically, λ_{CMI} governs the degree to which the conditional mutual information (CMI) loss is minimized. When $\lambda_{CMI} \leq 5$, we observed a modest increase in accuracy as the hyperparameter increases, accompanied by a uniformly decreasing trend in fairness violation. However, when $\lambda_{CMI} > 5$, further increments in λ_{CMI} lead to a decline in accuracy, even though the fairness violation continues to decrease. This behavior suggests that a moderate level of CMI minimization is beneficial in eliminating unwanted information from the latent code, yet an excessive emphasis on minimizing mutual information may inadvertently remove essential target information from z_Y .

Similarly, λ_{LRI} , which regulates the extent to which the latent code z_R captures correlated information, exhibits a comparable pattern. For $\lambda_{LRI} \leq 60$, an increase in λ_{LRI} results in an improvement in accuracy and a consistent reduction in fairness violation, indicating that a controlled increase enables z_R to capture sufficient shared patterns while mitigating conflicts between disentanglement and target prediction. Conversely, when $\lambda_{LRI} > 60$, the accuracy begins to decline, despite further reductions in fairness violation. This outcome implies that while a higher λ_{LRI} encourages z_R to absorb more correlated information and improves the overall disentanglement performance, it may also lead to the retention of excessive extraneous information, thereby compromising the integrity of the target information.

Fair Classification

The objective of fair classification is to achieve a balance between minimizing fairness violations and maintaining high predictive performance. To evaluate the effectiveness of our proposed method, we conduct experiments on a diverse set of benchmark fairness datasets. For facial attribute classification tasks, we utilize the CelebA (Liu et al. 2015) and UTKFace (Zhang, Song, and Qi 2017) datasets. Following prior works (Wang et al. 2022; Xu et al. 2020; Zeng et al. 2022; Jang and Wang 2024), we set the CelebA classification task to predict the "Smiling" attribute, while for UTKFace, the objective is to classify whether a person depicted in the image is over 35 years old, with gender serving as the sensitive attribute. Additionally, the Dogs and Cats dataset (Parkhi et al. 2012) is used to distinguish between dogs and cats, with fur color as the sensitive attribute. Furthermore, we assess fair classification performance using the Colored MNIST dataset (Kim, Lee, and Choo 2021; Kim et al. 2019; Nam et al. 2020), which incorporates a controlled color bias in the standard MNIST dataset to simulate spurious correlations. In this dataset, a fixed color is assigned to each digit for a majority of the training samples—specifically, 70% of the samples have each of the 10 digits correlated with one of 10 predefined colors (with a small random perturbation), while the remaining 30% are assigned colors uniformly among the other options. For the test set, every digit is paired with a uniformly distributed color assignment to eliminate bias. In our fair classification task, the digit serves as the target attribute and the color as the sensitive attribute. Originally introduced to measure the color bias of classifiers predicting digits, this setup is critical for evaluating a model's ability to disentangle the target digit information from the spurious color cues.

For model evaluation, we employ a 3-layered Multi-Layer Perceptron (MLP) classifier for all compared methods in all datasets. The input to the classifier consists of target-related features extracted from the pre-trained disentangled representations produced by each method. Specifically, we use z_Y of our method to feed into the classifier, while using z_X from FFVAE (Creager et al. 2019) and z_Y from FADES (Jang and Wang 2024). For invariant learning methods including FairFactorVAE (Kim and Mnih 2018), FairDisCo (Liu et al. 2022), GVAE (Ding et al. 2020), the entire latent space is utilized for downstream classification tasks. For non-adversarial learning method, we use z_T from ODVAE (Sarhan et al. 2020). This experiment setup represents different disentanglement learning strategies as detailed in the related works section. To assess fairness violations, we use standard metrics including Demographic Parity (DP) (Barocas and Selbst 2016) and Equalized Odds (EOD) (Hardt, Price, and Srebro 2016). Each method is evaluated over five experimental runs with different random dataset splits when the split is not predefined. This ensures robustness and statistical reliability in performance comparisons.

Demographic Parity (DP) is defined as:

$$DP = \left| \mathbb{P}(\hat{Y} = 1 \mid A = 0) - \mathbb{P}(\hat{Y} = 1 \mid A = 1) \right|, \quad (64)$$

where \hat{Y} denotes the predicted outcome and A represents the binary sensitive attribute (e.g., gender, race). This metric

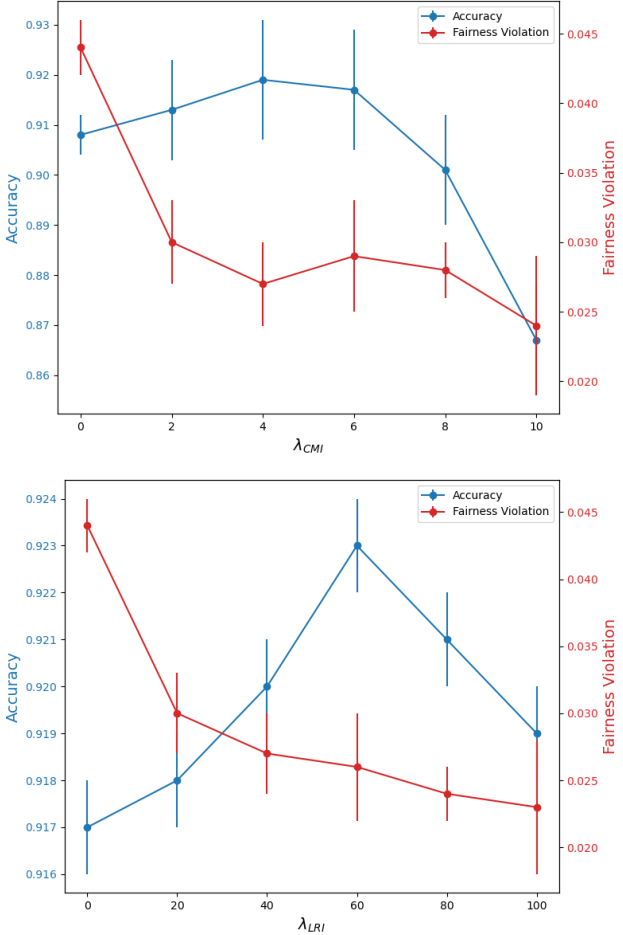


Figure 5: Top: Impact of varying λ_{CMI} (with λ_{LRI} fixed at 60) on classification accuracy and fairness violation (EOD) in the CelebA dataset classification task. Bottom: Impact of varying λ_{LRI} (with λ_{CMI} fixed at 5) on the same performance metrics.

captures the absolute difference in positive prediction rates across the groups.

Equalized Odds (EOD) requires that the predictor's true positive rates and false positive rates be equal across groups. It is defined as:

$$EOD = \max_{y \in \{0,1\}} \left| \mathbb{P}(\hat{Y} = 1 | Y = y, A = 0) - \mathbb{P}(\hat{Y} = 1 | Y = y, A = 1) \right|, \quad (65)$$

where Y represents the true outcome. This metric considers the maximum discrepancy over both outcome classes, ensuring fairness in both detection and error rates.

Fair Counterfactual Generation

To quantitatively assess the quality of the generated counterfactuals, we compare evaluation metrics between the direct reconstruction of the input image and the reconstructions obtained by randomly permuting the latent representations z_Y and z_S within the evaluation set. Specifically, we use the Fréchet Inception Distance (FID) (Heusel et al. 2017; Jang and Wang 2024) to assess reconstruction fidelity and the Inception Score (IS) (Chong and Forsyth 2020) to evaluate semantic and perceptual quality. Lower values of ΔFID indicate minimal distortion and higher translation quality, while lower values of ΔIS suggest that semantic and perceptual attributes are well preserved.

We first evaluate reconstruction fidelity by computing the FID between the original image set X and its reconstructed counterpart \hat{X}_{perm} , where the reconstruction is performed after a random permutation of the latent codes. Formally, we define

$$\Delta FID = FID(X, \hat{X}_{perm}), \quad (66)$$

where $X = \{x_i\}_{i=1}^N$ denotes the set of original input images and $\hat{X}_{perm} = \{\hat{x}_i^{perm}\}_{i=1}^N$ represents the corresponding reconstructed images. A lower ΔFID value implies higher translation quality, as it reflects minimal image distortion and fidelity loss during the counterfactual generation process.

In addition, we assess the semantic and perceptual quality by employing the Inception Score. The IS for the direct reconstruction is computed as

$$IS(X) = \exp(\mathbb{E}_{x \sim p(x)} [\text{KL}(p(y|x) \| p(y))]), \quad (67)$$

where $p(y|x)$ denotes the conditional probability distribution over labels given an image x , and $p(y)$ represents the marginal distribution over labels. Similarly, we compute $IS(\hat{X}_{perm})$ for the permuted reconstructions. The absolute difference between these scores is then defined as

$$\Delta IS = |IS(X) - IS(\hat{X}_{perm})|. \quad (68)$$

A lower ΔIS value indicates that the semantic and perceptual attributes of the image are well-preserved after translation, thereby validating the quality of the counterfactuals generated.

Together, these complementary metrics provide a comprehensive evaluation of the counterfactual generation quality. By quantifying both fidelity and semantic consistency, our experimental design rigorously validates the performance of the proposed method.

Fair Fine-Grained Image Editing

Similarly, we quantitatively assess the quality of fine-grained image editing by computing the differences in evaluation metrics between the direct reconstruction of the input image and the reconstructions obtained via latent code traversals with varying λ combinations. Specifically, we define

$$\Delta FID = FID(X, \hat{X}_{trav}), \quad (69)$$

and

$$\Delta IS = |IS(X) - IS(\hat{X}_{trav})|, \quad (70)$$

where $X = \{x_i\}_{i=1}^N$ denotes the set of original input images, and $\hat{X}_{trav} = \{\hat{x}_i^{trav}\}_{i=1}^N$ represents the corresponding reconstructed images obtained via latent code traversals.

In our experimental setup, where *Smiling* is the target attribute Y and *Gender* is the sensitive attribute S , we generate interpolated latent codes between source and reference images. Specifically, the interpolation is performed on the latent codes z_Y , z_S , and z_R . The interpolation parameters for z_Y and z_S are set to

$$\lambda \in \{0, 0.33, 0.66, 1\},$$

while for z_R the parameters are chosen from

$$\lambda \in \{0, 0.5, 1\}.$$

Thus, the overall combination of latent modifications involves $4 \times 4 \times 3$ distinct λ combinations, corresponding to different configurations for z_Y , z_S , and z_R . During each traversal, the latent code z_X remains unchanged, ensuring that the variations reflect only the task-relevant attribute transformations.

In this context, ΔFID measures the reconstruction fidelity, with lower values indicating that the traversed reconstructions closely resemble the original images in terms of their distribution. Likewise, ΔIS quantifies the preservation of semantic and perceptual quality; lower values suggest that the intrinsic content and visual features remain consistent despite the latent manipulations.

Additional Experiment

Fair Classification

To further validate the efficacy of our method in achieving fairness via effective disentanglement, we conducted additional experiments with different target attributes. Following the experimental setup in the main paper on the CelebA dataset, our evaluations extended beyond the "Smiling" attribute to include other widely adopted target labels, such as "Blond Hair", "Attractiveness" and "Young" under gender bias conditions. As summarized in Table 6, our method consistently achieves competitive accuracy while significantly mitigating fairness violations compared to existing approaches. These results further substantiate the robustness of our fair disentanglement learning strategy and demonstrate its applicability across a variety of target attributes.

Table 6: **Evaluation of downstream classification tasks on CelebA dataset for various target attributes from learned representation.** Best in **bold**, second in **red**.

Methods	CelebA Classification Performance											
	Smiling			Blond Hair			Attractive			Young		
	Acc ↑	EOD ↓	DP ↓	Acc ↑	EOD ↓	DP ↓	Acc ↑	EOD ↓	DP ↓	Acc ↑	EOD ↓	DP ↓
FADES (Jang and Wang 2024) [CVPR’24]	0.918	0.034	0.135	0.930	0.118	0.153	0.763	0.308	0.346	0.835	0.164	0.169
GVAE (Ding et al. 2020) [CVPR’20]	0.919	0.047	0.131	0.940	0.484	0.247	0.779	0.564	0.431	0.841	0.209	0.176
FFVAE (Creager et al. 2019) [PMLR’19]	0.892	0.076	0.072	0.926	0.301	0.201	0.749	0.359	0.310	0.832	0.281	0.195
ODVAE (Sarhan et al. 2020) [ECCV’20]	0.886	0.039	0.103	0.896	0.465	0.210	0.719	0.551	0.438	0.827	0.297	0.262
FairDisCo (Liu et al. 2022) [KDD’22]	0.839	0.074	0.051	0.916	0.465	0.234	0.750	0.515	0.411	0.839	0.226	0.196
FairFactorVAE (Liu, Sun, and Zhao 2023)	0.914	0.055	0.136	0.918	0.326	0.174	0.709	0.459	0.350	0.827	0.296	0.318
CAD-VAE (Ours)	0.923	0.021	0.112	0.939	0.105	0.137	0.773	0.268	0.290	0.847	0.151	0.155

Fair Counterfactual Generation

In this subsection, we present the results of counterfactual generation on the CelebA dataset (Liu et al. 2015). Figure 9 and Figure 10 display a grid of images, each row corresponding to a specific configuration of latent codes. The second row shows the direct reconstruction of the original input image, which is shown in the first row. The intermediate rows illustrate variations derived from different latent code substitutions. For instance, in the third row of Figure 9, the latent code configuration $[z_X^{(0)}, z_Y, z_S, z_R]$ is used, where the digit 0 indicates that the reference image is the one in the 0th column. In this configuration, the images in the subsequent columns are generated by replacing their latent code z_X with the z_X from the 0th column image, while the remaining latent codes (z_Y, z_S , and z_R) are retained. This approach effectively alters the corresponding features in the generated images. Our experiments demonstrate that both sensitive and target attributes can be distinctly translated. Moreover, the method supports the simultaneous translation of these attributes, thereby providing greater flexibility in generating counterfactuals. For instance, given an image of a smiling female, our approach can produce images representing a non-smiling male, a non-smiling female, and a smiling male, contributing to improved individual fairness (Jung et al. 2025) by ensuring that individuals with similar characteristics but different sensitive attributes receive comparable outcomes.

Fair Fine-Grained Image Editing

In this subsection, we display more fair fine-grained image editing results in Figure 6, following the experiment setup in the main paper. Specifically, as the correlated latent code z_R captures sensitive relevant information, we can explicitly control these properties: in the left subfigure, we gradually introduce makeup (such as enhanced lipstick and eyeshadow), while in the right subfigure, we progressively add a mustache.

t-SNE Visualization

To better understand the distribution and disentanglement of the learned representation, we present a t-SNE visualization analysis of the target latent code of each method. The visualizations are derived from experiments in Section 4.1 of the main paper where the model is trained on a biased color MNIST dataset and tested on an unbiased color MNIST dataset. Each figure consists of two subfigures: the left subfigure is colored according to the Digit attribute (target attribute),

and the right subfigure is colored according to the Color attribute (sensitive attribute). Clear and distinct clustering in the left subfigure indicates that the model has learned a robust and discriminative representation of the target attribute, thereby enhancing its recognizability. Conversely, if the right subfigure exhibits discernible color clusters, it suggests a correlation between the target and sensitive attributes, indicating weaker disentanglement performance. A uniform color distribution in the right subfigure, however, confirms that the sensitive information has been effectively filtered out.

This visualization in Figure 7 demonstrates that our proposed method effectively disentangles the learned representation. The target attribute (Digit) exhibits distinct, well-separated clusters with clear classification boundaries and a pure distribution, while the sensitive attribute (Color) is uniformly distributed and unrecognizable. This confirms that our method achieves superior separation of the target attribute without introducing unwanted bias from the sensitive attribute.

Text-to-Image Editing

To further validate the capability and explore the applicability of our method, we integrated it as an adaptor on top of a pre-trained, frozen CLIP image encoder (Radford et al. 2021) and trained it on datasets including CelebA (Liu et al. 2015) and Facet (Gustafson et al. 2023) to enhance fairness in vision-language tasks. Table 7 and Table 8 present the experimental results on CelebA and Facet, respectively. These results demonstrate that our approach significantly improves fairness without compromising performance compared to the linear probing baseline (ERM), underscoring its potential for a range of vision-language tasks such as search and image retrieval with fairness considerations.

In Table 8, we also present an ablation study that examines the contribution of each loss term, as detailed in the last three rows. Each row represents training using only L_{ELBO} , without L_{CMI} , and without L_{LRI} , respectively.

Table 7: **Performance of CLIP(ViTB/32) on CelebA dataset.**

Method	Acc ↑	EOD ↓	DP ↓
Zero-shot	0.857	0.834	0.715
Linear prob	0.918	0.924	0.837
CAD-VAE	0.921	0.037	0.133

Furthermore, we applied our method in StyleCLIP (Patashnik et al. 2021) as a fair discriminator to address inherent

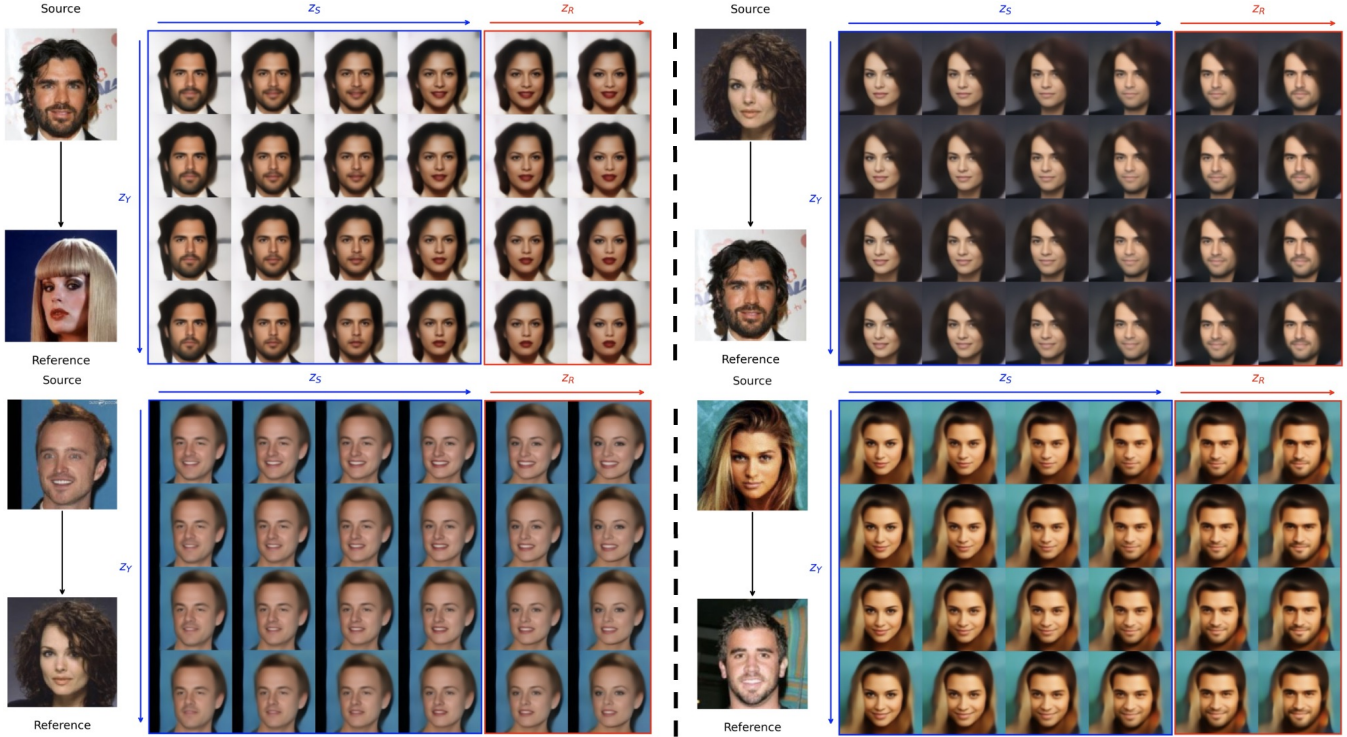


Figure 6: Examples of Fair Fine-Grained Image Editing. Zoom in to check. The leftmost column shows the source and reference images. The blue-framed section displays images generated by interpolating z_Y and z_S (with z_R and z_X fixed), where the horizontal axis varies z_S and the vertical axis varies z_Y . The red-framed section illustrates images produced by interpolating z_Y and z_R (with z_S fully replaced by the reference and z_X constant). Modification in one latent code minimally affecting others, harness z_R to edit sensitive relevant feature(makeup or mustache).

fairness issues, such as career-gender biases, which persist even when an identity preservation loss is employed. As illustrated in Figure 8, StyleCLIP (Patashnik et al. 2021) exhibits a bias by correlating the role of “dancer” with a specific gender. In contrast, our method effectively mitigates this bias while maintaining the efficacy of attribute modification.

Limitation and Future Works

The limitations of our work can be summarized in two main aspects. First, while our study addresses the inherent trade-off between fairness and performance under certain data biases, fairness violations can arise from a variety of sources. CAD-VAE specifically mitigates the unwanted correlation between sensitive attribute and target attribute, which represents one primary cause of fairness issues. However, in real-world applications, additional factors such as under-representation, intrinsic model bias, and the presence of missing or noisy features often co-occur, exacerbating fairness violations. Future research should aim to extend our theoretical framework to encompass these diverse and often overlapping sources of bias. Second, our current approach requires the availability of both target and sensitive attribute information during training. In many practical scenarios, acquiring such labeled data can be challenging due to high annotation costs or legal and regulatory restrictions. A promising direction for future work is to develop methods that relax this dependency, potentially through unsupervised or semi-supervised techniques, to learn

fair and disentangled representations without explicit reliance on labeled sensitive information.

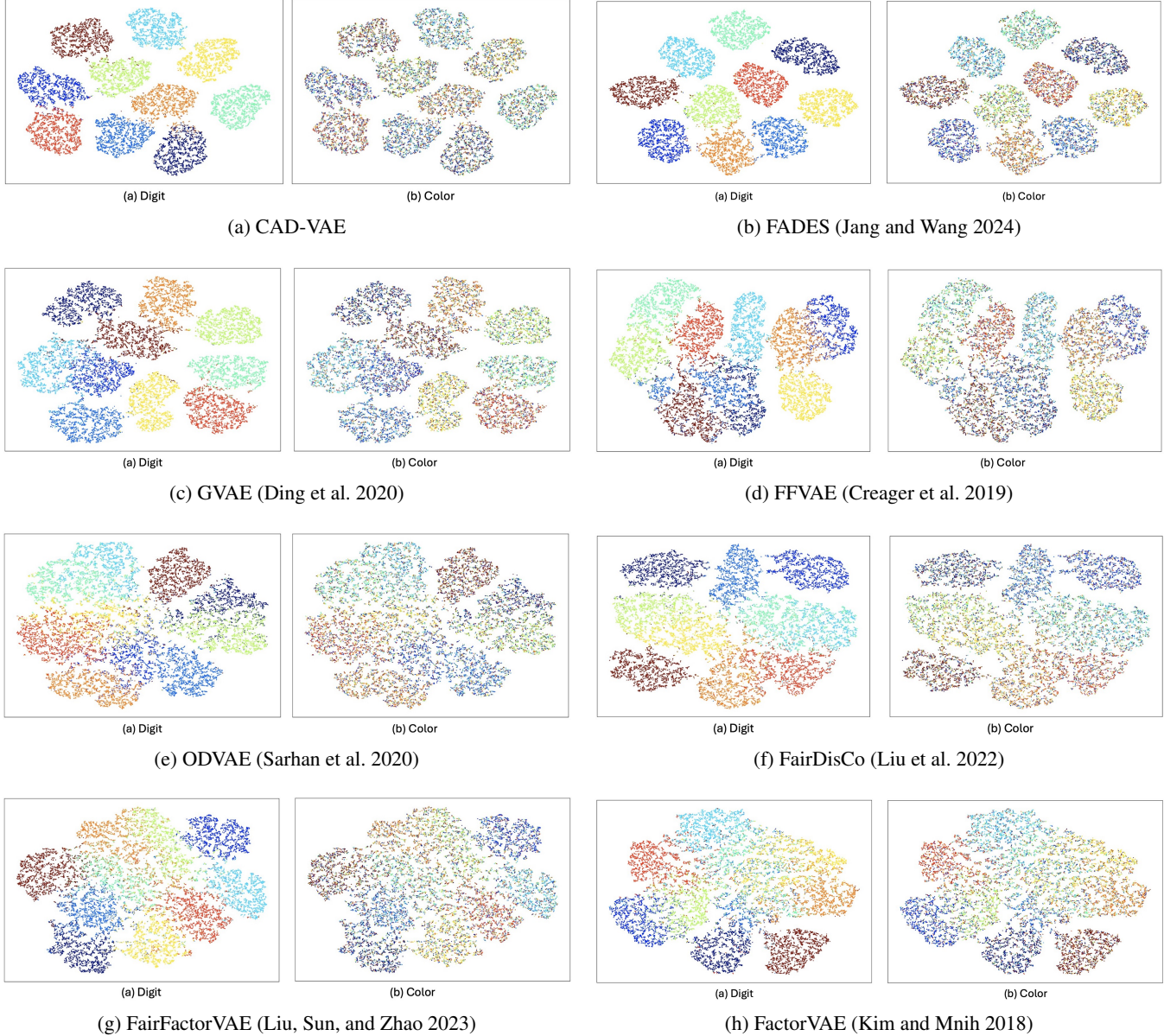


Figure 7: **t-SNE visualization of the target code from the test set for each method.** Left subfigure is colored by Digit; right subfigure is colored by Color.

Table 8: **Performance of CLIP(ViTB/32) on Facet dataset.** WG: Worst Group, Gap: Difference between WG and Avg.

Method	Top-1 Acc. (%)			Top-3 Acc. (%)		
	WG ↑	Avg ↑	Gap ↓	WG ↑	Avg ↑	Gap ↓
Zero-shot	2.79	53.45	50.66	15.31	76.79	61.48
Linear prob	1.17	65.46	64.29	1.79	85.34	83.55
CAD-VAE	69.97	70.54	0.57	85.36	85.95	0.59
(Abl.) $\mathcal{L}_{\text{ELBO}}$	16.34	67.27	50.93	37.24	86.96	49.72
(Abl.) w/o \mathcal{L}_{CMI}	20.43	67.67	47.24	25.41	91.12	65.71
(Abl.) w/o \mathcal{L}_{LRI}	24.03	64.19	40.16	29.17	87.42	58.25



(a) Original (b) StyleCLIP (c) StyleCLIP+

Figure 8: **Style transfer using StyleCLIP and the CAD-VAE extension.** This example transforms the (a) into “a dancer with long blonde hair.” “StyleCLIP+” means StyleCLIP + CAD-VAE.

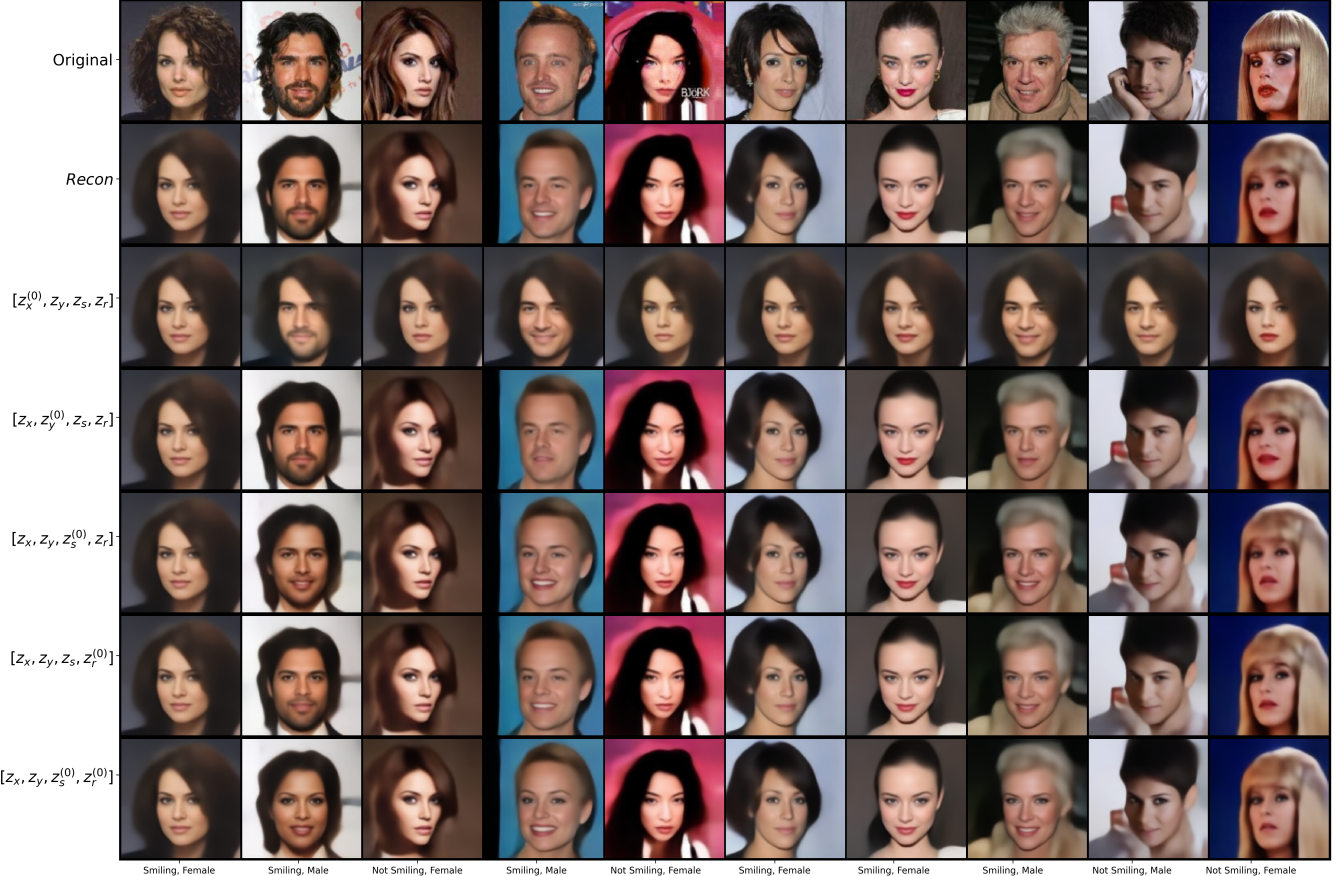


Figure 9: **Examples of Fair Counterfactual Generation.** The image in the 0th column serves as the reference, while the images in the remaining columns are the source images.

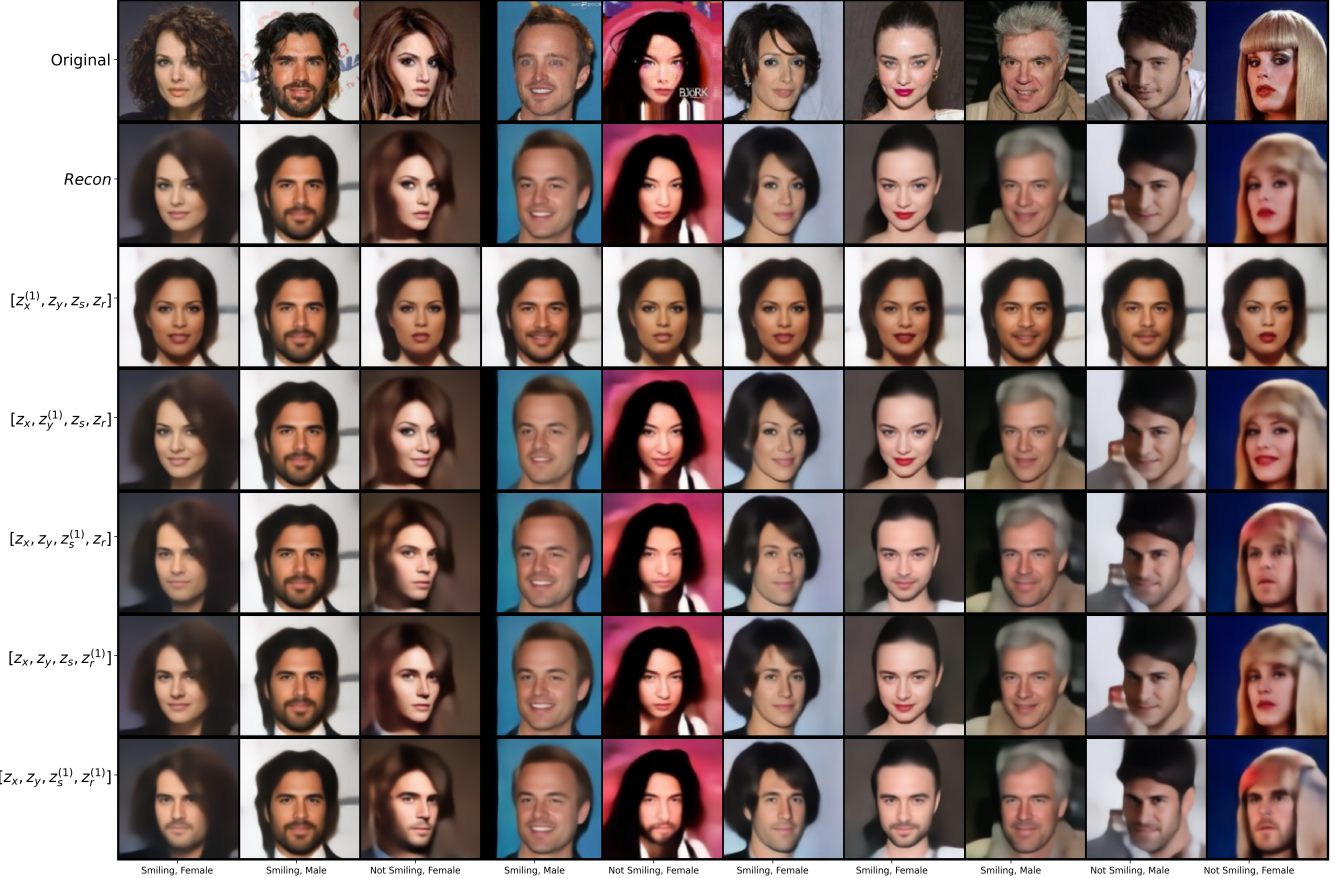


Figure 10: **Examples of Fair Counterfactual Generation.** The image in the 1th column serves as the reference, while the images in the remaining columns are the source images.